PROPAGATION OF HIGH-ENERGY LASER BEAM IN THE ATMOSPHERE

Charles B. Hogge

Air Force Weapons Laboratory
Kirtland Air Force Base, New Mexico

June 1974

AFWL-TR-74-74

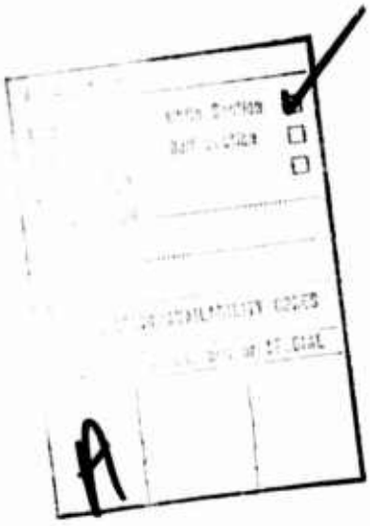

AIR FORCE WEAPONS LABORATORY
Air Force Systems Command
Kirtland Air Force Base
New Mexico 87117

When US Government drawings, specifications, or other data are used for any purpose other than a definitely related Government procurement operation, the Government thereby incurs no responsibility nor any obligation whatsoever, and the fact that the Government may have formulated, furnished, or in any way supplied the said drawings, specifications, or other data, is not to be regarded by implication or otherwise, as in any manner licensing the holder or any other person or corporation, or conveying any rights or permission to manufacture, use, or sell any patented invention that may in any way be related thereto.

DO NOT RETURN THIS COPY. RETAIN OR DESTROY.

UNCLASSIFIED
Security Classification

AD-781763

DOCUMENT CONTROL DATA - R & D

(Security classification of title, body of abstract and indexing annotation must be entered when the overall report is classified)

1 ORIGINATING ACTIVITY (Corporate author) Air Force Weapons Laboratory Kirtland AFB, NM 87117	2a. REPORT SECURITY CLASSIFICATION UNCLASSIFIED 2b. GROUP

3 REPORT TITLE

PROPAGATION OF HIGH-ENERGY LASER BEAM IN THE ATMOSPHERE

4 DESCRIPTIVE NOTES (Type of report and inclusive dates)
September 1972 - June 1973

5 AUTHOR(S) (First name, middle initial, last name)

Charles B. Hogge

6 REPORT DATE June 1974	7a. TOTAL NO OF PAGES 65	7b. NO OF REFS 55
8a. CONTRACT OR GRANT NO b. PROJECT NO 3326 c. Task 09 d.	9a. ORIGINATOR'S REPORT NUMBER(S) AFWL-TR-74-74 9b. OTHER REPORT NO(S) (Any other numbers that may be assigned this report)	

10 DISTRIBUTION STATEMENT

Approved for public release; distribution unlimited.

11 SUPPLEMENTARY NOTES	12 SPONSORING MILITARY ACTIVITY AFWL (ALO) Kirtland AFB, NM 87117

13 ABSTRACT

(Distribution Limitation Statement A)

Atmospheric turbulence can affect the propagation of laser beams of any power. Thermal blooming, a nonlinear propagation process, can seriously degrade high-energy beams. These two processes are reviewed in detail, with emphasis on parametric effects such as aperture size wavelength, and focal distance. Included in the discussion are such new topics as supersonic slewing and stagnation zone problems.

DD FORM 1 NOV 65 1473

UNCLASSIFIED
Security Classification

14 KEY WORDS	LINK A		LINK B		LINK C	
	ROLE	WT	ROLE	WT	ROLE	WT
Propagation Thermal Blooming Linear Propagation Turbulence						

AFWL-TR-74-74

PROPAGATION OF HIGH-ENERGY LASER BEAMS IN THE ATMOSPHERE

Charles B. Hogge

Final Report for Period September 1972 - June 1973

Approved for public release; distribution unlimited.

ic

FOREWORD

The research was performed under Program Element 62601F, Project 3326, Task 09.

Inclusive dates of research were September 1972 through June 1972. The report was submitted 4 March 1974 by the Air Force Weapons Laboratory Project Officer, Dr. Charles B. Hogge (AL).

This report is the lecture presented by the author at Physics of Quantum Electronics Short Course, Crystal Mountain, Washington, July 1973.

This technical report has been reviewed and is approved.

Charles B. Hogge

CHARLES B. HOGGE
Project Officer

ARMAND D. MAIO
Lt Colonel, USAF
Chief, Optics Branch

JOHN C. RICH
Lt Colonel, USAF
Chief, Advanced Laser Technology Division

ABSTRACT

(Distribution Limitation Statement A)

Atmospheric turbulence can affect the propagation of laser beams of any power. Thermal blooming, a nonlinear propagation process, can seriously degrade high-energy beams. These two processes are reviewed in detail, with emphasis on parametric effects such as aperture size, wavelength, and focal distance. Included in the discussion are such new topics as supersonic slewing and stagnation zone problems.

CONTENTS

ILLUSTRATIONS

ILLUSTRATIONS (Cont'd)

ILLUSTRATIONS (Cont'd)

SECTION I

INTRODUCTION

When laser radiation is transmitted through the atmosphere, numerous physical processes can occur that, generally speaking, alter the nature of the beam. When the power in the beam is low, the processes tend to be linear in nature. At high powers, new processes are found to occur. Depending on the specific application, these processes may limit the usefulness of the laser system.

In this report two phenomena characteristic of high-energy laser beams which propagate through the atmosphere are discussed. The first subject is atmospheric turbulence, a phenomenon which affects both high- and low-power beams. A brief introduction to the atmospheric effects that are the source of optical degradations is given. Next, certain theoretical implications of the propagation of focused beams are described. Finally, experimental observations that have been made on this aspect of propagation in a turbulent atmosphere are given.

The second subject is the thermal blooming of high-energy laser beams. Particular emphasis is placed on 10.6μm systems and the particular kinetic processes associated with the absorption of this wavelength in the atmosphere. A discussion of the current status of theoretical calculations is given and examples of the parameter dependencies of the phenomena are shown. The propagation of pulsed laser systems is discussed and results of some recent work presented.

SECTION II

LASER BEAM PROPAGATION IN ATMOSPHERIC TURBULENCE

1. BACKGROUND

When a laser beam traverses a distance in the atmosphere, its ideal phase characteristics experience small perturbations which alter and redirect the energy in the beam (refs. 1, 2, 3, 4, and 5). The resulting intensity fluctuations are called scintillations and have been observed when looking at twinkling stars. The source of these perturbations is a random index of refraction field. The source of this field is related through the density almost exclusively to temperature fluctuations. Pressure variations (P) are very small and are rapidly dispersed. One can therefore show that the change in the index of refraction with temperature (T) in the atmosphere (using an isobaric assumption) is given by

$$\Delta n(r) = - 79 \times 10^{-6} \frac{P}{T^2} \Delta T(r) \tag{1}$$

It is generally assumed that the atmosphere is at least locally homogeneous and isotropic, although this is often not true. To help diminish the problems associated with this assumption, atmospheric scientists often studied structure functions. Defined as

$$D_n(r_1,r_2) = \langle [(n(r_1)-\langle n(r_1)\rangle)-(n(r_2)-\langle n(r_2)\rangle)]^2 \rangle \tag{2}$$

where the brackets denote ensemble average, this function has been found to be less sensitive in form to the conditions of local homogeneity and isotropy. Assuming homogeneous and isotropic turbulence, the temperature field has been shown experimentally and theoretically for sufficiently small spacings (r) to have the form

$$D_T(r) = \langle (\Delta T(p) - \Delta T(r+p))^2 \rangle = C_T^2 r^{2/3} \tag{3}$$

Using high-speed temperature-sensitive instruments one can calculate the constant C_T (ref. 6). Through equation 1 a similar spatial dependence of the index of refraction can be obtained and hence a determination of C_n^2 made.

$$C_n^2 = \left(\frac{79P}{T^2}\,10^{-6}\right)^2 C_T^2 \qquad (4)$$

C_n^2 is frequently called the atmospheric structure constant, although it is seldom very constant. It has come to typify in one all-encompassing term the nature or strength of the atmospheric turbulence. Its value near sea level ranges from $10^{-17}m^{-2/3}$ or smaller for very weak turbulence to $10^{-13}m^{-2/3}$ or larger for very strong turbulence. Actually, the nature of atmospheric turbulence is much too complicated to be described very well by this one parameter. Notably, scale sizes are very important in the description of naturally occurring turbulence.

Temperature fluctuations are introduced into the atmosphere by large scale phenomena such as heating of the earth's surface. These disturbances are broken up and mixed by the wind until temperature fluctuations of all scale sizes exist. Wind fluctuations control the temperature variations. Hence, it is instructive to discuss the characteristics of the atmospheric wind field.

This field obtains energy from large scales such as wind shear or convection from solar heating of the ground. Therefore, the turbulence energy must be introduced by scale sizes larger than some minimum value (L_o) called the outer scale of turbulence. (Wave number $K_o = 2\pi/L_o$ in figure 1. Actually, figure 1 shows the power spectrum of the index of refraction fluctuations, but the form of the curve is equivalent to the velocity field power spectrum as well.) For $K < K_o$, the form of the power spectrum is not known in general, owing to its dependence on local conditions and surface terrain. In this region the turbulence is most likely not homogeneous and isotropic. Typical sizes for L_o vary from a number such as the height above ground to 100 meters or more for the upper atmosphere, although stratification can alter this. In figure 1, the inclusion of a finite outer scale causes the power spectrum to remain finite as $K \to 0$.

Under the assumptions that energy is input at the small wave numbers and dissipated at large wave numbers, and that for these scale sizes of turbulence the Reynolds number is much greater than unity, and that the scale sizes are small enough so that buoyancy forces are negligible, Kolmogorov originally

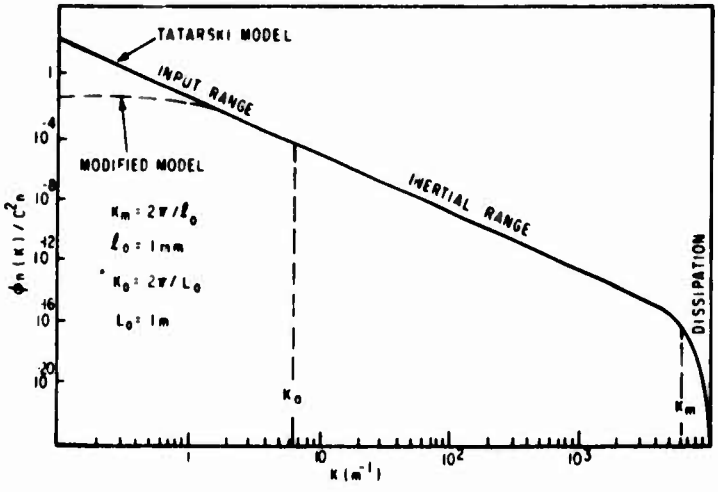

Figure 1. Three-dimensional Spectrum of the Refractive Index Fluctuations (ref. 4).

proposed a turbulence model that predicted a $K^{-11/3}$ spectrum in the inertial subrange where the scale sizes are smaller than L_0 but larger than ℓ_0; this has been experimentally verified. ℓ_0 is an inner scale length which marks the turbulence scale sizes for which viscous dissipation converts the energy in the turbulence into heat. Typically it is on the order of 1 mm near the ground to a few millimeters at altitude. In this region of the turbulence spectrum, the form is again not well known. However, it is clear that for $K > K_m = 5.92/\ell_0$, the slope of the spectrum is steeper than the slope of the inertial subrange.

It has been found that the temperature fluctuations obey the same spectral law as the velocity fluctuations. That is not to say that their magnitudes are related, however. Strong mechanical turbulence (i.e., velocity fluctuations) tends to smooth out temperature variations and produce an atmosphere with an adiabatic lapse rate. On the other hand, an atmosphere with very little wind can sustain very strong thermal gradients. For optical propagation, temperature is the primary source of disturbance.

Tatarski (ref. 1) used the following form for the power spectrum of the refractive index:

$$\Phi_n(K) = 0.033C_n^2K^{-11/3}\exp(-K^2/K^2m) \qquad (5)$$

This spectrum is singular at $K = 0$ and therefore does not possess a covariance function. This difficulty can be circumvented by use of a Von Karman spectrum of the form (ref. 4)

$$\Phi_n(K) = \frac{0.033 C_n^2 \exp(-K^2/K_m^2)}{(K^2 + (L_o/2\pi)^{-2})^{11/6}} \qquad (6)$$

that artificially imposes a well behaved dependence for $K \to 0$.

In figure 2 some experimental results are presented to show (ref. 7) the simultaneous behavior of the measurement of optical intensity scintillation and and C_n^2. Plotted on the ordinate is the variance of the log amplitude $\sigma_\chi^2 = \langle(\chi - \langle\chi\rangle)^2\rangle$, where $\chi = \ln(A/A_o)$, A_o and A being the unperturbed and perturbed field amplitudes, respectively (note $I \sim A^2$, where I is the field irradiance). The theoretical log amplitude variance prediction for a spherical wave source in turbulence is

$$\sigma_\chi^2 = 0.124\, C_n^2\, Z^{11/6}\, k^{7/6}$$

where $k = 2\pi/\lambda$, λ is the optical wavelength, and Z is the range to the observation plane. These results show the good agreement between macroscopic measurements of turbulence and simultaneous optical effects. Note the increased strength of both processes during daylight hours, the very low values at sunrise and sunset, and the nighttime variability. The two simultaneous optical path

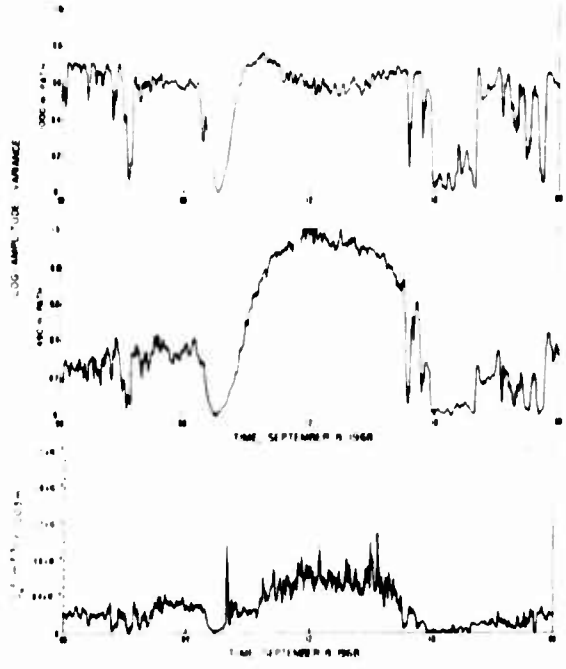

Figure 2. Simultaneous Amplitude Scintillation and Turbulence Structure Constant Data (ref. 7).

measurements also show the frequently referred to phenomenon of saturation of scintillation (refs. 8, 9, 10, and 11); during daylight hours, the variance of log irradiance of the 1000-m path is actually lower than the same quantity measured in the 490-m path. This behavior has frequently been observed and is really only understood in principle to be a multiscattering phenomenon.

2. PROPAGATION OF BEAM WAVES IN A TURBULENT ATMOSPHERE

Historically, one finds that much of the original experimental and theoretical work has been directed to studying the propagation effects of plane and spherical wave sources in a turbulent medium. In recent years there has been considerable interest in extending the earlier theories to treat the propagation of beam waves in turbulence. The theoretical work has been extensive (refs. 12 through 20) and presents many interesting questions which need to be tested by the experimentalist. Unfortunately, experimental results on beam wave propagation have been slow in developing (refs. 22 through 27) owing mainly to the difficulties associated with good quality large laser optics and related instrumentation. The remaining discussion of atmospheric turbulence effects will be confined to those results which specifically apply to the propagation of beam waves. (A beam wave may be defined as any transmission configuration which does not fall in the spherical wave or plane wave propagation case. Stated slightly differently, it may be defined as a propagation arrangement in which the transmitted beam emerges from optics which have finite size.)

Consider an experimental arrangement (figure 3) in which a beam wave is transmitted through atmospheric turbulence to a target where it is observed. The transmitter characteristics are specified by the output beam diameter (D), the wavelength (λ), and the focal length (F). The intervening turbulence is specified by the structure constant (C_n^2) and the outer and inner scale sizes. If $L_o > D$, then there must be turbulence scale sizes that are larger than the beam diameter at all points along the beam path. These "turbules" act as week lenses which deflect the beam as a whole in a random way leaving the shape of the beam unaltered. This is called beam wander. Scale sizes smaller than the diameter of the beam diffract and refract the beam and generally smear out its energy distribution profile, an effect referred to as beam breathing and scintillation. Depending on the characteristics of the turbulence and the transmitter, these two mechanisms share with some proportion in producing the total average long term distortion of the beam.

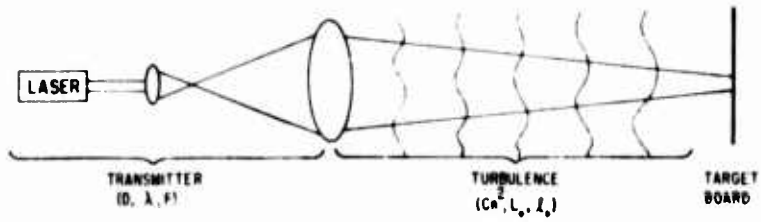

Figure 3. Usual Propagation Configuration.

Kerr (ref. 23) has observed that under moderate strengths of turbulence, the focal plane distribution retains its diffraction-limited beam size but moves randomly mainly under the influence of the large turbulence scale sizes (figure 4). He has observed large scintillation effects, however, at points well removed from the central spot of the beam. The reduction in scintillation of the central spot is predicted in one beam wave theory (ref. 12), but the same theory apparently fails to adequately account for the beam wander effects (ref. 23). This theory also predicts a severe sensitivity of scintillation of focus adjustments, an effect which Kerr found to be true (figure 5). Misadjustments in focus resulted in a beam which scintillated strongly in the form of many time-evolving intensity blobs each of which is approximately the size of the transmitter's diffraction limit. In the presence of strong turbulence, the beam breaks up into a proliferation of many spots, each of which is also approximately the spot size of the transmitter's diffraction limit (figure 6). In this situation, the phase distortions incurred by the beam are so large that the physical concept of focus no longer seems to be valid.

A problem closely related to the propagation configuration of figure 3 is shown in figure 7. If one observes the image plane characteristics of the point source, one will find almost exactly the same characteristic dependences as Kerr found for the beam wave projected through the turbulence. This is no accident, and it is related to the reciprocity of the linear turbulence operator.

For example, beam wander is clearly a major concern in the propagation of beam waves, for there exists the possibility that this phenomenon can be removed by fast tracking optical systems. Because the beam wander is mainly a result of large turbulence scale sizes, geometrical optics approaches to the problem should yield good results. Many persons have attempted this approach making a special treatment of turbulence scale sizes which are larger than (or smaller) than the beam size (refs. 24 and 26). Hull, et al. (ref. 24), using such an approach, obtained the following expression for the angular beam wander (along one axis)

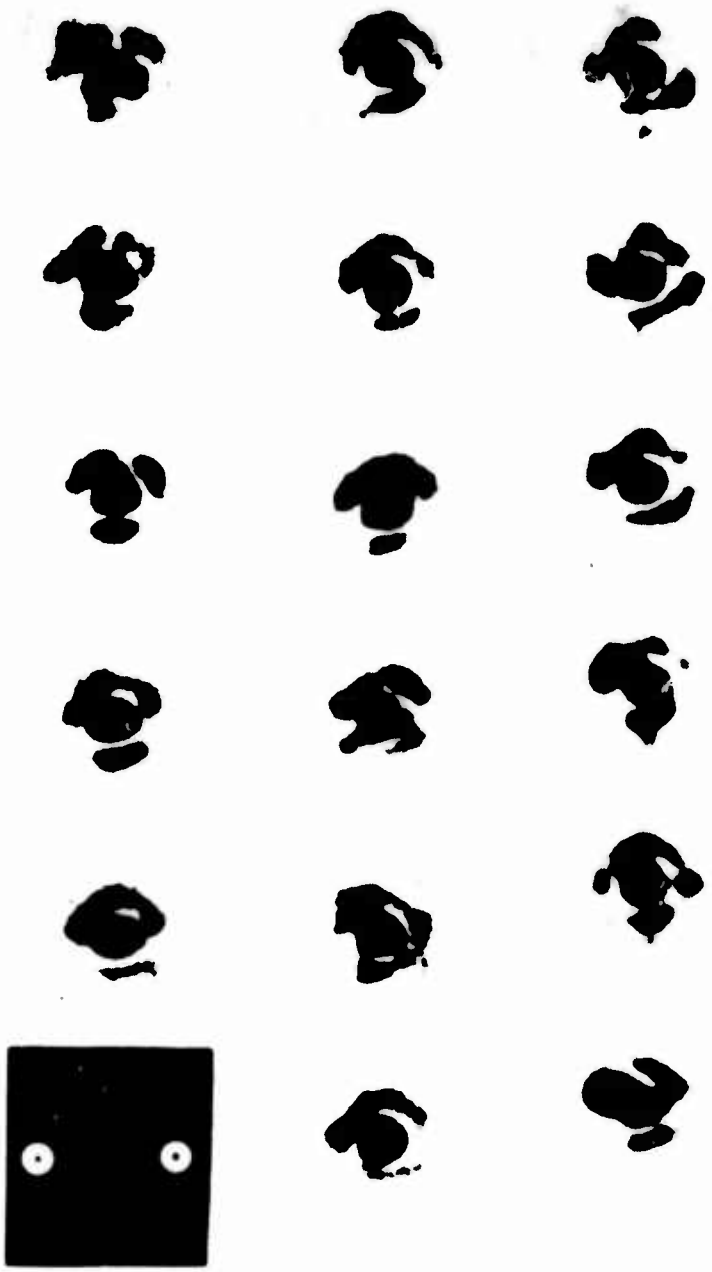

Characteristic received beam for a focused, near-field transmitter in moderate turbulence. The duration of each frame was 4 ms; the time between adjacent frames was 21 ms. The frame sequence is downward in each column, and the scale marks represent 2.5 cm. $\lambda = 4880$ Å, $L = 1.4$ km, $D_t = 15$ cm, $\alpha_1 L = 0.09$.

Figure 4. Focal Plane Irradiance Distributions in Moderate Turbulence (ref. 23).

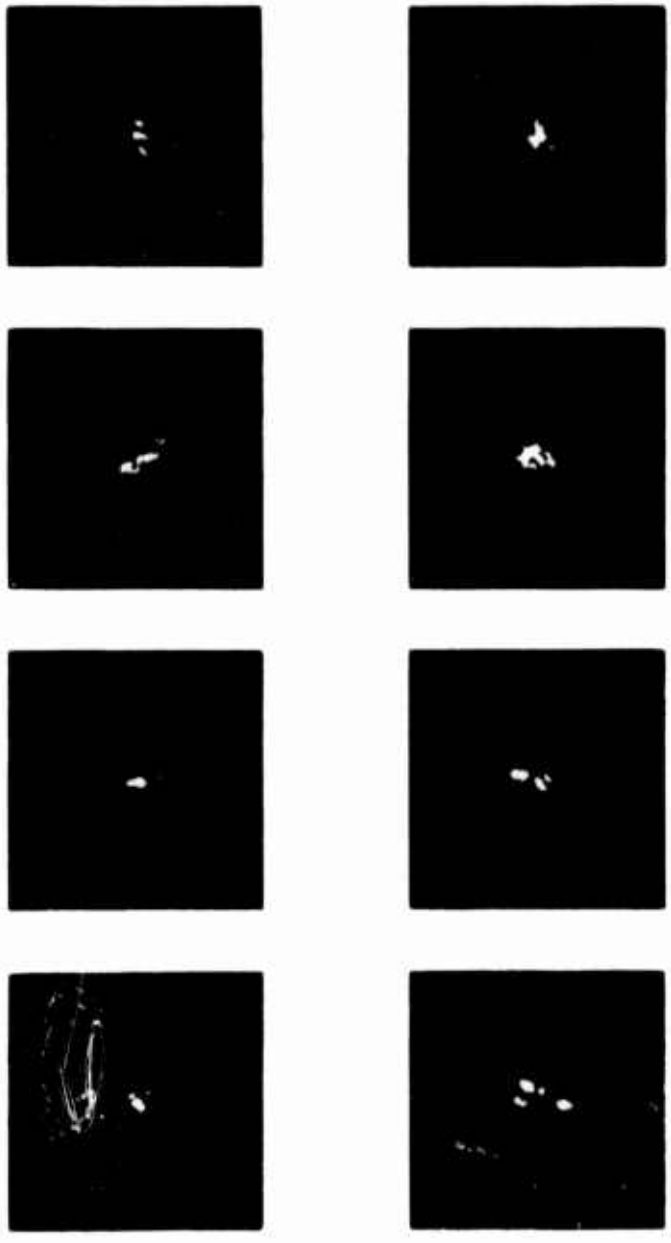

Received beam vs transmitter focal adjustment for the near field transmitter of Fig. 1 in moderate turbulence. Successive frames clockwise represent axial focal adjustments of 50 μm compared to an effective focal length of 120 cm. Precise focus is illustrated in the third frame. Individual patches have the same nominal size as the central spot in Fig. 1.

Figure 5. Irradiance Distribution Characteristics as a Function of Focus Setting (ref. 23).

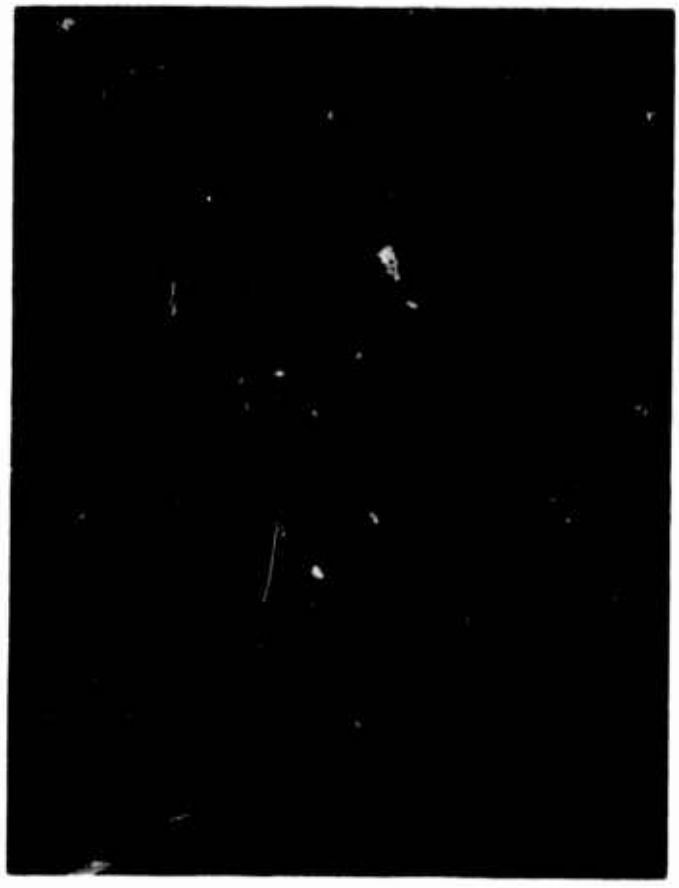

Received beam for the focused, near field transmitter of Fig. 1 in strong turbulence. Individual patches have the same nominal size as the central spot in Fig. 1

Figure 6. Typical Irradiance Distribution in the Focal Plane for Strong Turbulence (ref. 23).

Figure 7. Reciprocal Propagation Configuration.

$$\langle\alpha^2\rangle = \frac{3}{4} LD^{-1/3}C_n^2 \left\{1.46 - \frac{8}{9}(D/L_o)^{1/3}\right\} \quad (7)$$

Considering the reciprocal problem (figure 7) several other persons have analyzed the nature of the focal plane image dancing (refs. 3, 15, 16, 20, and 27). Fried (ref. 27), for instance, used an approach that decomposed the turbulence distorted phase profile at the collecting aperture into a series of polynominals. He then defined the angle of arrival as the angle normal to the best fit linear plane surface through the phase aberrations. Heidbreder (ref. 16), also using an extremum approach, defined the angle formed in the direction of maximum instantaneous power as the beam wander. Both workers arrived at identical results for image dancing (ref. 20).

In the limit $L_o \to \infty$, they obtained (for spherical waves)

$$\langle\alpha^2\rangle = (2.91)(3/8)(1.026)L(D)^{-1/3}C_n^2 \quad (8)$$

which differs from equation 7 by about 1 percent. The thrust of the image-dancing analysis can be easily visualized in the following argument originally proposed by Hufnagel (ref. 19). Consider an arbitrary phase distribution across an aperture of diameter D. The phase difference between opposite points on the edge of the aperture is $[\phi(D/2,0) - \phi(-D/2,0)]$ so that the angular tilt is just

$$\alpha = [\phi(D/2,0) - \phi(-D/2,0)]/kD \quad (9)$$

where $k = 2\pi/\lambda$. Assuming a zero mean for α, one gets for the variance

$$\langle\alpha^2\rangle = D_s(D)/k^2D^2 \quad (10)$$

where $D_s(\cdot)$ is the phase structure function. For a spherical wave, and $L_o \to \infty$, and $D \sim \sqrt{\lambda L}$

$$\langle\alpha^2\rangle = (2.91)(3/8)LD^{-1/3}C_n^2 \quad (11)$$

which is quite similar to equation 8. Inclusion of outer scale effects produces

$$\langle\alpha^2\rangle = (2.91)(3/8)LD^{-1/3}C_n^2(1-0.67(D/L_o)^{1/3}) \quad (12)$$

where $\mathcal{L}_0 = L_0/2\pi$. The existence of a finite outer scale tends to decrease the strength of the beam wander (ref. 14).

Beam wander has been measured by a few researchers under varying conditions of transmitter configuration and turbulence strengths (refs. 22 23, 24, 26, and 28). Some of the most interesting work was performed by Dowling, et al., at NRL, where they simultaneously measured through common optics the far-field irradiance characteristics of laser radiation of two very different wavelengths (0.6328μm and 10.6μm). Their results show, among other things, that beam wander is to a very high degree independent of wavelength (figure 8) as the theory predicts and a reasonably accurate function of LC_n^2 (figure 9). Maximum values of $\langle\alpha^2\rangle$ exceeded $1.6 \times 10^{-8}\mu rad^2$ at times of strong turbulence.

The developments leading to equations 7, 8, 11, and 12 stress the importance of the phase structure function. To include amplitude effects, the wave structure function, defined as the sum of the phase and log amplitude structure functions, should be used instead. However, for many situations of interest, the effects of phase aberrations strongly outweigh the comparable amplitude effects and can be shown to dominate the far-field distributions. Nonetheless, it should be kept in mind that these developments have assumed small amplitude disturbances. In any event amplitude effects should never produce more than a factor-of-two effects in the calculations.

The reciprocity of beam wander (figure 3) and image dancing (figure 7) is only part of a very useful reciprocity theorem. It may be stated as follows (ref. 29). Consider a single realization of the random index of refraction field between two points in space ($\underline{p}_1$ and $\underline{p}_2$). The field at point $\underline{p}_1$ due to a unit amplitude spherical wave source at point $\underline{p}_2$ is exactly the same as the field at $\underline{p}_2$ due to a unit amplitude spherical wave source at point $\underline{p}_1$. Any linear refractive element (say for example, a lens) may be placed between $\underline{p}_1$ and $\underline{p}_2$, and the reciprocity theorem is still valid.

Two important results are implied by the point-to-point reciprocity therein. First, one can show that if the instantaneous phase and amplitude distribution can be measured in the transmitting aperture for point source located at the receiver plane, then by transmitting a beam whose amplitude and phase is exactly conjugate to this, the far field irradiance distribution is limited only by the diffraction aspects of the telescope. This is to say, all the deleterious effects of the intervening turbulence can be eliminated. Of course, it is no simple feat

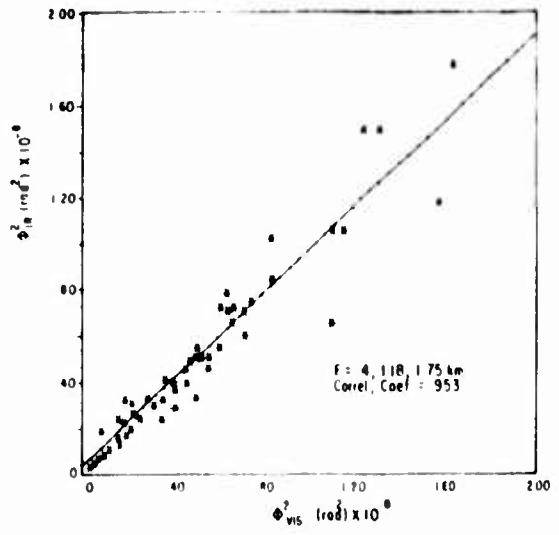

Figure 8. Experimental Beam Wander Data for a Visible and an Infrared Beam (ref. 22).

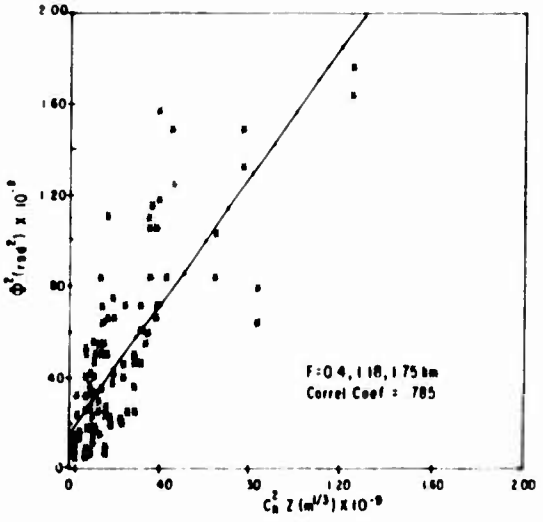

Figure 9. Experimental Beam Wander as a Function of C_n^2 Z (ref. 22).

to either instantaneously measure the amplitude and phase of the point source accurately or to quickly and precisely generate a beam with the conjugate field distribution. However, there does exist the possibility of rapidly sensing (through heterodyne detection, for instance) an effective wave front tilt for the spherical wave. Transmitting a beam with the conjugate tilt (fast tracking telescopes do this) can eliminate the beam wander component of the phase distortion.

A second result of the point-to-point reciprocity theorem is the following. If a lens is used to collect and image a point source that is imbedded within the turbulence, then for every instant in time there will be a certain random irradiance distribution obtained in the receiver's focal plane. If at that same instant in time one could use the collecting telescope as a transmitting telescope, in a reciprocal configuration, then the irradiance distribution thus obtained would be precisely the same as the one obtained in the imaging configuration. This suggests, among other things, that for the determination of the wavefront tilt, one need only observe the angular deflection of the image of the point source. Thus, a collecting telescope and a displacement detector (such as a quad cell, for instance) can make a very simple device for rapidly sensing wavefront tilting.

These two results follow from the point-to-point reciprocity theorem, but in reality they only approach the exactness implied above when a certain condition is satisfied. That condition requires that the refractive scattering of the turbulent medium must be weak enough to insure that the focal plane spot size of the transmitted beam including beam wander and beam spreading must be smaller than the isoplanatic patch size. The meaning of this isoplanatic patch size can be illustrated as follows. Suppose two point sources are imbedded in the turbulent medium adjacent to one another. In the focal plane of the receiving telescope, the two sources will be imaged side by side. If the two images are exactly alike (and this of course requires some qualification), then the two point sources are said to be within the isoplanatic patch size. The focal plane spot size of the transmitted beam will be within the isoplanatic patch if the invariance of the two point source images is maintained for lateral separations larger than the focal plane beam diameter. For strong optical distortions, the isoplanatic assumption may be violated, vitiating the two previous results; nonetheless, point-to-point reciprocity will still be valid under any condition. Incidentally, the isoplantic requirement is usually satisfied for most optical systems operating in the near field of the transmitting aperture. In addition,

it can be shown that the isoplanatic qualification can be totally removed if one considers statistical quantities, such as the long time averaged size of the beam.

Using this theorem, Lutomirski and Yura (refs. 13 and 31) have developed an elegant propagation theory which seems to coalesce nicely with the few recorded experimental observations of beam wave propagation which are available for detailed comparison. Hufnagel and Stanley (ref. 19), Fried (ref. 18), and Mooreland and Collins (ref. 17) developed a similar line of analysis for the case of an imaging receiver. By the reciprocity theorem, they are now known to be the same. Lutomirski and Yura show that the irradiance at a point $\underline{p}$ in the receiver plane is given by (ref. 13)

$$I(\underline{p}) = \left(\frac{k}{2\pi Z}\right)^2 \iint \exp\{ik(s_1 - s_2)\}$$

$$\cdot \exp\{\Psi(\underline{r}_1) + \Psi^*(\underline{r}_2)\}\, U_A(\underline{r}_1)\, U_A^*(\underline{r}_2) d\underline{r}_1^2 d\underline{r}_2^2 \qquad (13)$$

where $U_A(\underline{r})$ is the transmitted aperture distribution; s_1, s_2 are the geometric distances between points $\underline{p}$ and the points $\underline{r}_1$ and $\underline{r}_2$ in the aperture, respectively; and, $\Psi(\underline{r}_1)$ and $\Psi(\underline{r}_2)$ are the perturbations in the field at $\underline{p}$ due to unit spherical waves emitted at $\underline{r}_1$ and $\underline{r}_2$.

Performing an ensemble average, or as is done in practice, averaging over a time long compared to all the beam wander and beam scintillation frequencies of interest, one gets

$$\langle I(\underline{p})\rangle_{LT} = \left(\frac{k}{2\pi Z}\right)^2 \iint \exp[ik(s_1 - s_2)] M_s^{LT}(\underline{r}_1, \underline{r}_2, Z)$$

$$\cdot U(\underline{r}_1) U^*(\underline{r}_2) d^2\underline{r}_1, d^2\underline{r}_2 \qquad (14)$$

where M_s^{LT} is the "long time" mutual coherence function of a point source located at the receiver plane and measured at the transmitter plane. One can readily show that if $\Psi(r_1) = \chi + iS$, where $\chi = \ln (A/A_0)$ (A_0 being the unperturbed amplitude of the field and A the perturbed amplitude) and where S is the perturbation to the phase, then assuming that the random quantities are Gaussian random variables,

$$M_s^{LT}(\rho,z) = \langle \exp(\psi(\underline{r}_1)\ \psi^*(\underline{r}_2))\rangle = \exp\{-D(\rho)/2\} \tag{15}$$

where $|\underline{r}_1 - \underline{r}_2| = \rho$ and where $D(\rho)$ is the wave structure function given by

$$D(\rho) = D_X(\rho) + D_S(\rho) \tag{16}$$

Homogeneous and isotropic turbulence has been assumed. In terms of the covariance function (instead of structure functions)

$$D(\rho) = 2(B(0) - B(\rho)) \tag{17}$$

$B(0)$ is a constant and is equal to the sum variances of the log amplitude fluctuations and the phase fluctuations. $B(\rho)$ is the covariance function which can assume many forms but in general has the property that as $\rho \to \infty$ $B(\rho) = 0$. Thus a typical form for the mutual coherence function in equation 14 might be like the function shown in figure 10. Lutomirski and Yura show that the asymptotic limit is given by

$$B(0) = 2Z/Z_c \tag{18}$$

where

$$Z_c = \left[2\pi^2 k^2 \int_0^\infty \Phi_n(K) K dK\right]^{-1} \tag{19}$$

for $\ell_o << L_o$, equation 19 can be approximated by

$$Z_c \approx (0.4k^2 C_n^2 L_o^{5/3})^{-1} \tag{20}$$

Notice that in the limit of infinitely large L_o (as implied by the power spectrum of equation 5), $Z_c = 0$. This is a reflection of implication that there is, in this limit, an infinite amount of energy in the turbulence spectrum, which of course is not true. Nonetheless, if one holds all else constant, then by increasing the outer scale size the total energy in the turbulence spectrum grows, and hence more severe optical effects occur. Thus, it is valid to conclude that when equation 5 can be used to calculate optical quantities, the results generally form an upper limit estimate of the effects. This is illustrated in the comments that

follow. Z_c has units of length and may be thought of as designating a propagation distance for which the mean field of a spherical wave is reduced by e^{-1} from its vacuum value.

For homogeneous and isotropic turbulence, equation 14 can be written in the paraxial approximation as

$$\langle I(\underline{p})\rangle = \left(\frac{k}{2\pi Z}\right)^2 \iint d^2\underline{\rho} M_s^{LT}(\underline{\rho},z)\exp[-(ik/z)\underline{\rho}\cdot\underline{p}]$$

$$\iint U(\underline{r}+\underline{\rho}/2)U^*(\underline{r}-\underline{\rho}/2)\exp[(ik/z)\underline{\rho}\cdot\underline{r}]d^2r \qquad (21)$$

where the second double integral can be identified as the modulation transfer function (MTF) of the transmitter. This function varies in shape dependence on the nature of the telescope and radiation source but generally might have a shape as shown in figure 10 (bottom curve). As the diameter of the transmitted beam is increased, or the wavelength of the radiation shortened, the cut-off frequency grows larger indicating an increase in the resolution of the telescope (and conversely, indicating a decrease in the transmitted diffraction limited spot size).

Consequently, equation 21 can be interpreted as stating that the MTF of the total system (atmosphere and telescope) is the product of the MTF of the atmosphere and the MTF of the telescope. The irradiance distribution (point spread function) is just the Fourier transform of the total system MTF.

Clearly, if $M_s^{LT}(\underline{p}) = 1$, (for all $\underline{p}$), the system will be diffraction limited, the integral argument being dominated by the MTF of the telescope. In fact, if $\exp[-B(0)]$ is greater than e^{-1}, for example, the effects of turbulence on the optical transmission characteristics are very slight. If, however, $\exp\{-B(0)\} \ll e^{-1}$, the atmosphere has a strong effect on the beam. The degree to which the effect is severe depends critically on the width of $M_s^{LT}(\rho)$. Lutomirski and Yura arbitrarily define a (long term) "coherence diameter" as being that value of $\rho=\rho_0$ for which $M_s^{LT}\left(\rho_0^{LT}\right) = e^{-1}$. In order to be able to do this, one must require of the propagation range being considered that $M_s(\ell_0,Z) \simeq 1$ and $M_s(L_0,Z) \ll 1$ which implies that

$$Z_c \ll Z \ll Z_i \qquad (22)$$

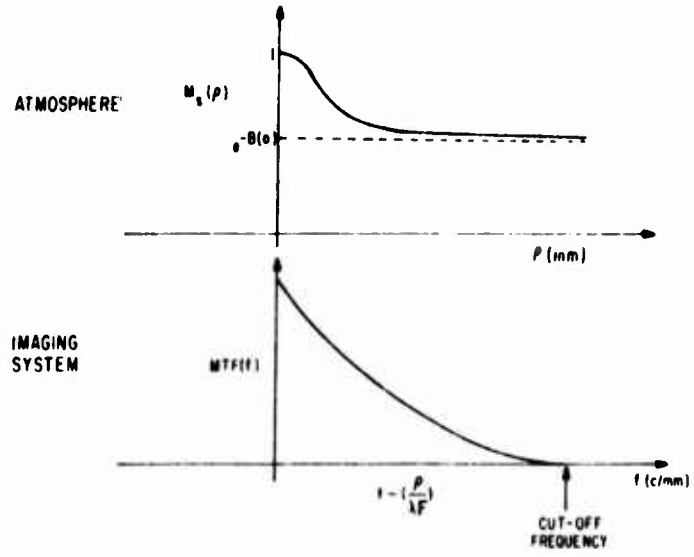

Figure 10. Typical Modulation Transfer Functions for the Atmosphere and for a Telescope.

where $Z_i = Z_c(L_o/\ell_o)^{5/3}$. In this region, one can write approximately that

$$M_s^{LT}(\rho,z) = \exp[-1.4(Z/Z_c)(\rho/L_o)^{5/3}(1-0.71(\rho/L_o)^{1/3}] \tag{23}$$

$$\rho_o^{LT}(LT) \simeq \rho_o^{LT}(\infty)(1 + 0.426[\rho_o^{LT}(\infty)/L_o]^{1/3}) \tag{24}$$

where $\rho_o(\infty) = (0.545\ ZC_n^2k^2)^{-3/5}$ is the coherence diameter obtained by assuming an infinitely large outer scale (i.e., using equation 5 for the power spectrum).

If $Z >> Z_i$, then $M_s^{LT}(\ell_o,Z) << 1$ and the focal plane irradiance distribution is very broad. The $M_s^{LT}(\rho)$ is found there to depend most strongly on the inner scale characteristics:

$$M_s^{LT}(\rho) = \exp[0.8(Z/Z_i)(\rho/\ell_o)^2] \tag{25}$$

For this case,

$$\rho_o = [0.76\ C_n^2Z^{1/2}\ell_o^{-1/6}k]^{-1} << \ell_o \tag{26}$$

One can then interpret the preceding results as follows. Turbulence converts a coherent radiator of diameter D into a partially coherent radiator diameter

ρ_0^{LT}. The size of ρ_0^{LT} is determined solely by the mutual coherence function (MCF) of a spherical wave source located at the receiver and measured in the transmitter plane. Incidentally, to be more precise, in the range where $Z_c \leq Z \leq Z_i$, and $L_0 \to \infty$, ρ_0 is given by the following weighted integral.

$$\rho_0^{LT} \simeq \left[1.45k^2 \int_{Z_1}^{Z_2} C_n^2(Z') \left[\frac{Z_2 - Z'}{Z_2 - Z_1}\right]^{5/3} dZ'\right]^{-3/5} \tag{27}$$

This implies that the turbulence near the transmitter (Z_1) is weighted most heavily as affecting the beam propagation characteristics. Thus, for instance, if atmospheric turbulence can be assumed to decrease with altitude, then ground-based illuminators of airborne receivers are degraded more seriously than equivalent airborne illuminators of ground-based receivers.

The relative size of ρ_0^{LT} to D has been found to correlate well with the observations made by Kerr (ref. 23). The following conclusions apply to a beam focused in the near field of the transmitting aperture. Namely, when $\rho_0 >> D$, no turbulence effects of any degree are significant. For $\rho_0^{LT} \approx D$, beam wander is found to be the predominant propagation effect, with very little instantaneous beam breathing or scintillation. For $\rho_0^{LT} \leq D$, beam wander is still a major effect, but now beam breathing is becoming a competing process, although still not dominant. If $\rho_0^{LT} << D$, scintillation, and beam spreading are the dominant effects.

Amplitude scintillation effects are small when Z is in the near field of the ρ_0^{LT} or D, whichever is smaller; i.e., $Z \leq k \rho_0^{LT^2}$. (This condition coincides nicely with the requirement that the amplitude scintillation of a spherical wave remain small.) For $Z > k\rho_0^{LT^2}$, where $\rho_0 << D$ the beam breaks up into a proliferation of individual patches of spots, each approximately the diffraction spot size of the transmitting aperture. Focusing in this case ceases to have a well-defined meaning.

One implication of the preceding which is important is that when $Z \lesssim Z_c$, substantial improvement in far field irradiance can be achieved by using increasingly larger transmitting optics (ref. 16). This conclusion however, does not follow if the power spectrum of equation 5 is used. In that case, the MCF is found to be given by

$$M_S(\rho) = \exp[-(2.91)(3/8)k^2C_n^2Z\rho^{5/3}] \qquad (28)$$

which rapidly tends to an asymptotic value of zero for large ρ, (i.e., $Z_C \to 0$ as $L_0 \to 0$ as noted before). Recalling the form of the calculation of the irradiance distribution, the quantity of interest is the product of the atmospheric and telescopic MCF's. If the aperture of the transmitter is made sufficiently larger and larger, its MCF becomes wider than the atmospheric MCF (figure 10), so that the integral in equation 21 is determined solely from the form of the latter MCF. When equation 28 is used for the form of the atmospheric MCF, this implies that the maximum far-field irradiance achievable with increasingly larger transmitting optics is limited (See figure 11 from ref. 16.). With the inclusion of outer scale effects, and the assumption that $2Z/Z_C \lesssim 1$, the correct form of the atmospheric MCF shows an asymptotic limiting values as $\rho \to \infty$ of $\exp(-2Z/Z_C)$. The area under this curve grows without limit (conceptually) so that by making the MCF of the telescope broader ($D \to \infty$), the far field irradiance can be continually (and substantially) improved (figure 11). For values of $Z/Z_C \gg 1$, the differences in the shapes of the atmospheric MCF's became less significant, with the result that for all practical purposes the maximum irradiance in the far field does saturate with increasing transmitting aperture diameter.

Recently Yura (ref. 15) has developed a similar formalism to describe "short time" propagation effects. These effects include only the average instantaneous beam characteristics, beam wander being filtered out of the long time atmospheric MCF. Yura's results follow from the development of the short time MCF (due to Fried, ref. 18) and really apply only when scintillation effects are small. One determines that

$$M_S^{ST}(\rho) = \exp\left\{-\left(\frac{\rho}{\rho_0^{LT}}\right)^{5/3}\left[1-0.62(\rho/D)^{1/3}\right]\right\} \qquad (29)$$

where this is valid when $\rho \gg (\lambda Z)^{1/2}$, $L_0 = \infty$ (and consequently for $Z_C \lesssim Z \lesssim Z_I$). Proceeding as before, one can define an approximate short time lateral coherence diameter as

$$\rho_0^{ST} = \rho_0^{LT}\left[1 + 0.37(\rho_0^{LT}/D)^{1/3}\right] \qquad (30)$$

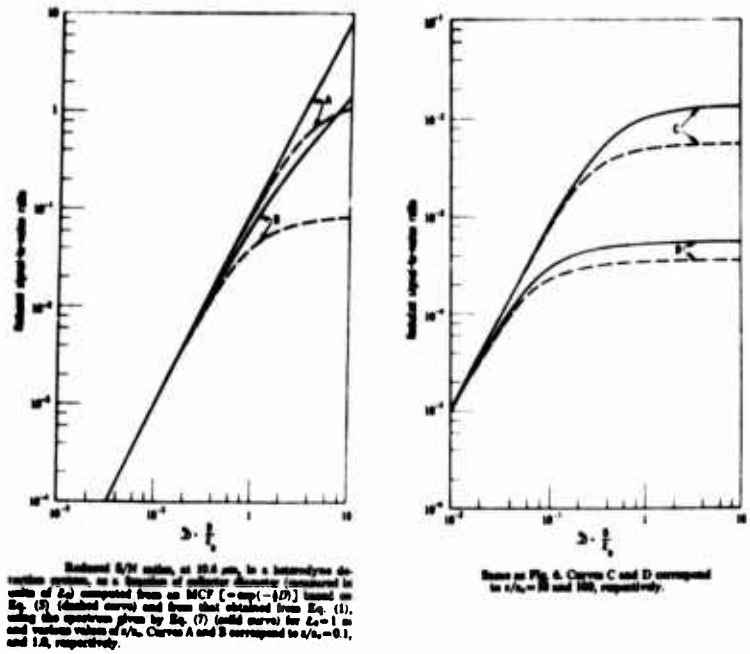

Figure 11. Transmitter Aperture Dependence in Turbulence (ref. 31).

The implications are that if one can track out (or in some other manner remove) the beam wander, the effective atmospheric MCF is broadened, with a subsequent increase in the effective coherence diameter of the radiator. One might then alter the preceding interpretation of the experimental results by replacing everything that was said about ρ_0^{LT} by ρ_0^{ST}. The fact of the matter is, however, that these parameters do not differ greatly anyway, so that the thrust of the argument is still very much the same.

Yura (ref. 30) also shows that one can obtain an approximate estimate for the size of the irradiance distribution (defined to the e^{-1} point) as

$$p_I^2 = p_0^2 + p_T^2$$

where

$$p_0 = \frac{2Z}{kD}$$

and

$$p_T = \frac{2Z}{k\rho_0^{LT}} \text{ or } \frac{2Z}{k\rho_0^{ST}}$$

depending on the specific problem of interest. One can then make an argument for the approximate independence of the beam wander and beam spreading processes and assert that the two random effects can be root-mean-squared (rms) as

$$\langle \alpha^2 \rangle = (p_{LT}^2 - p_{ST}^2)/Z^2 \qquad (32)$$

which can be compared with the work described earlier for beam wander. The agreement in functional dependence is exact, but they differ in magnitude by about 20 percent, the latter angular variance being smaller. This is probably a reflection of the inappropriateness of the rms assumption, although this has not been shown.

In equation 29, it is clear that as $D \to \infty$, the long time and short time effects cease to be different. Physically this corresponds to situations where the transmitting aperture size is larger than almost all the turbulence scale sizes of interest. Spatial averaging of the turbulence over the width of the beam only produces beam spreading, beam wander becoming a secondary effect. In view of this observation and with the possibility of tracking out beam wander, the curves in figure 11 now appear as shown in figure 12. Removing beam wander can produce a system with an optimum far-field irradiance that is larger than the large aperture limiting value. Subsequent increase in transmitting aperture size actually leads to a decrease in system performance (although very slowly).

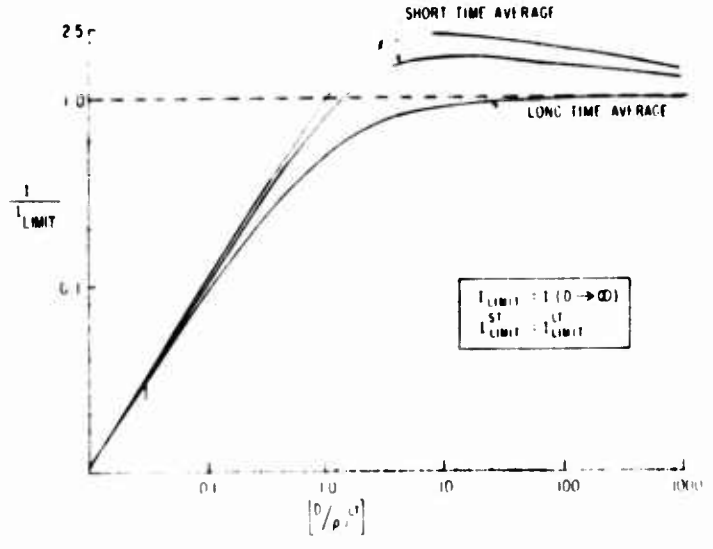

Figure 12. Average Focal Plane Maximum Irradiance Dependence on Transmitter Aperture Size, for Long-term and Short-term Averages.

The two upper curves utilize the two different beam wander approaches, Yura's approach being the lower of the two. The lowest curve not exceeding the asymptotic value is the same as the curves shown in figure 11 with $L_0 \to \infty$.

The wavelength dependence in this problem has not been mentioned. Clearly beam wander is a wavelength-independent phenomenon; however, beam spreading is not, and it does exhibit a weak theoretical wavelength dependence. To illustrate the dependence, consider two systems. Both systems are operating with the same total output power, transmitter diameter, focal length setting, and wavelength of radiation. The first system does not have the ability to track beam wander, whereas the second system does, and this is their only difference. Pose the following problem: if one is at liberty to alter the wavelength of the source radiation, what transmitting aperture size will produce the same far field irradiance maxima? The results for the first system are shown in figure 13. In the absence of turbulence, the dashed line indicates the appropriate system and therefore the ideal aperture. With turbulence, however, one finds that one needs apertures which are slightly larger than the ideal limit, indicating that turbulence is affecting the shorter wavelengths more severely. In addition, there is a limiting wavelength, below which no finite aperture can achieve the equivalent irradiance (again the case where $Z \to Z_c$ has been used).

When beam wander is removed, one observes a similar behavior shown in figure 14. Note that since wander has been removed, these curves represent an effectively higher maximum irradiance, and yet, the optimum wavelength is actually less than for the long time average case. The explanation for this is related to the fact that beam wander is not wavelength dependent. Consequently, the effect of a particular value of beam wander on the far-field irradiance is proportionally larger for the shorter wavelength system. Of course, all of these conclusions assume that the observation plane is in the near field of the spherical wave lateral coherence diameter in order to assure small amplitude scintillation effects.

It might be pointed out that this curve is not asymptotic at this apparent value of wavelength. Actually, with increasing transmitter diameter, the corresponding system equivalent wavelength begins to increase again, eventually asymptoting a wavelength that is larger than the limiting wavelength in figure 13. This is to be expected, since the curves in figure 14 correspond to a higher system equivalent irradiance than the ones in figure 13. The limiting intensity

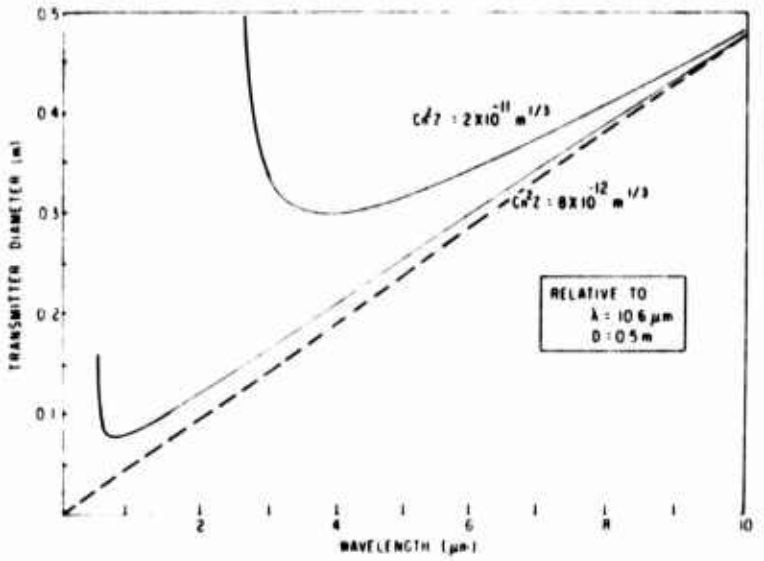

Figure 13. Equivalent Transmitting Systems That Produce Constant Focal Plane Maximum Intensity for Different Strengths of Turbulence (Long-term Average).

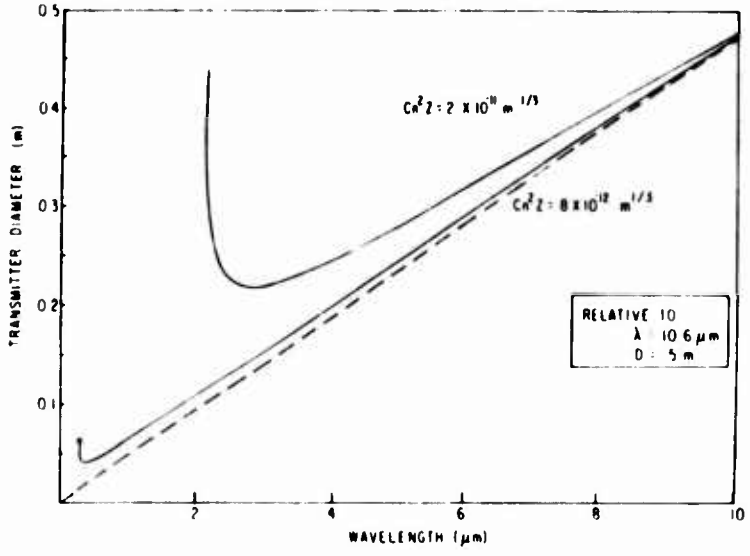

Figure 14. Equivalent Transmitting Systems That Produce Constant Focal Plane Maximum Intensity for Different Strengths of Turbulence (Short-term Average).

as $D \to \infty$ can be easily shown to vary as $\lambda^{2/5}$, and therefore a longer wavelength system is needed in order to achieve the proportionally higher irradiance value obtained by tracking out beam wander.

Thus, even though there is only a weak dependence on the radiation wavelength, its inclusion in the turbulence problem can in some situations strongly alter the final system design considerations.

SECTION III

LASER BEAM PROPAGATION IN AN ABSORBING MEDIUM

1. BACKGROUND

The propagation of laser beams in turbulence is a linear process in that the medium is not perturbed by the presence of the radiation. Strictly speaking, this is only true for very low power beams. As the energy is increased, absorption of the radiation begins to induce temperature changes in the medium, which in turn, result in density, and therefore index of refraction changes. These then alter the optical characteristics of the medium. The process is nonlinear, in that the beam irradiance distribution induces index of refraction changes in the medium that in turn alters the beam irradiance characteristics, which alters the refractive index changes, etc.

In the past, one basic problem has received a great deal of attention in the open literature (refs. 32 through 42). Specifically, the following assumptions were usually made with regard to the thermal blooming problem: (1) the high-energy beam has an unperturbed irradiance profile that is Gaussian in shape; (2) the medium through which the beam passes is flowing at a constant velocity that is much less than the speed of sound and is free of any turbulence (i.e., laminar flow); (3) the beam is assumed to have been "on" for a time long enough to establish a steady state irradiance distribution; (4) the wavelength of the radiation is 10.6 μm; and (5) it has been assumed that the energy thermalization process produces an instantaneous heating of the medium. In addition, using assumption 2, it can be shown that the hydrodynamic processes of interest are essentially isobaric, and therefore an instantaneous temperature change in the medium causes an instantaneous density change and, therefore, refractive index change.

In this section the nature of the results obtained for the basic thermal blooming problem described by the assumptions above is discussed. In addition, some recent work on related subjects will also be presented. The discussion begins with a brief review of the basic thermal blooming problem.

2. BASIC PROBLEM CONSIDERATIONS

With the five assumptions specified above, the thermo-optical process is conceptually easy to visualize. Figure 15 is a simplified description of what is known as pure blooming. Holding assumption 2 in abeyance for the moment, assume that the air is stationary, so that at t = 0 second, the temperature, density, and index of refraction profile are constant across the beam. When the beam has been turned on, some of the radiation energy is absorbed and then released in the form of heat in the gas; the temperature in the vicinity of the beam rises. Air mass subsequently flows away from the beam center (at the speed of sound) lowering the index of refraction. The beam then experiences a weak defocusing effect much the same as a negative lens. Frequently an annular irradiance distribution appears in some planes away from the transmitter plane. This has been demonstrated experimentally and typical results are shown in figure 16 (frame two, numbered from left to right, and top to bottom). These pictures were obtained by passing a 10.6 μm laser beam through a CO_2 filled absorption cell. The latter four pictures were obtained by translating the beam laterally through the cell, thereby simulating a wind.

The effect of a wind on pure thermal blooming is shown in figure 17. As a parcel of air moves across the beam, it absorbs energy, causing a temperature rise. Again, mass flows away from the parcel at the speed of sound, decreasing its density. As a result, the density and therefore refractive index profile across the beam both tend to decrease from the upwind to the downwind side. The light rays, bending into more (optically) dense regions, are therefore refracted into the wind. In figure 16, the wind direction is downward in frames 3 to 6. Note that for slower wind speeds, a crescent-shaped irradiance distribution occurs. At higher wind speeds, the parcel of air is carried through the beam so rapidly that very little energy can be deposited during the time that it is in the vicinity of the beam. Density changes are thus very small, and consequently, very little optical distortion occurs. The transit time of a parcel of air across the beam is a characteristic time of interest to the thermal blooming problem. For times less than this number, thermal blooming (beam divergence in frame 2 of figure 16) is the main source of optical distortion. For times long compared to the transit time, a steady state irradiance distribution evolves.

Another characteristic time of importance to thermal blooming is the sound speed transit time across the beam (also called the acoustic transit time, t_{ac}).

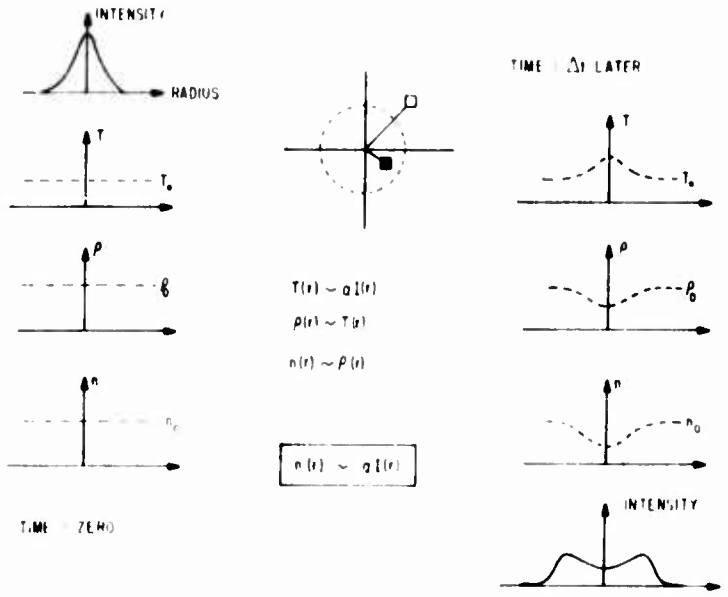

Figure 15. Simplified Graphical Description of Thermal Blooming in Quiescent Air.

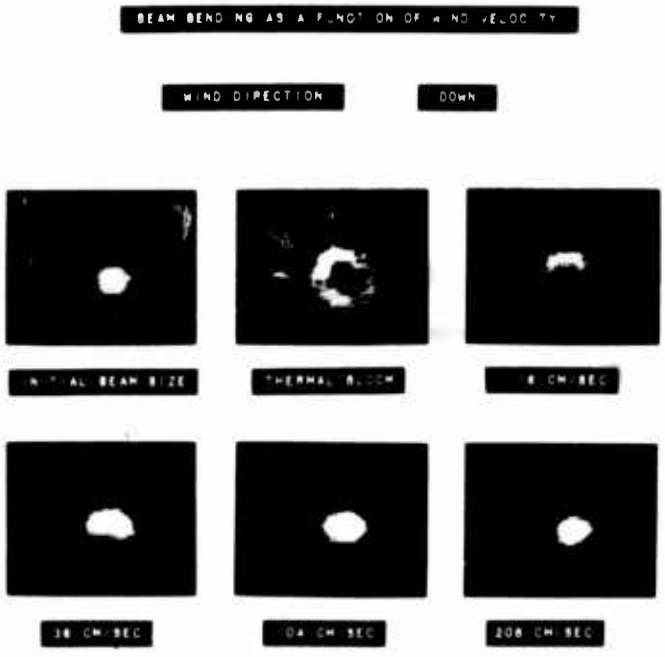

Figure 16. Experimental Data Describing Thermal Blooming and Beam Bending for Various Transverse Wind Speeds.

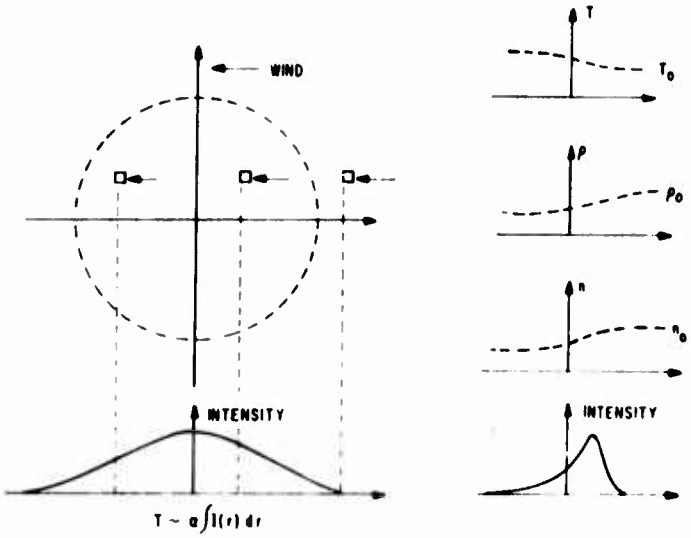

Figure 17. Simplified Graphical Description of Thermal Beam Bending for a Constant Transverse Wind.

Temperature disturbances in a gas cause pressure disturbances that are rapidly dispersed as sound waves. At standard temperature pressure (STP), the speed of sound is approximately 330 m/sec. For times long compared to the acoustic transit time, the isobaric assumption of the hydrodynamic processes is valid. In times short compared to this, computation of transient density changes is no longer isobaric and requires special treatment. This is a time regime of interest in high-energy laser pulse propagation.

For the record, the parabolic wave equation is generally used for the thermal blooming problem.

$$\nabla_T^2 U - 2ikn_0 \frac{\partial U}{\partial Z} + k^2(n^2-n_0^2)U = 0 \qquad (33)$$

where $[U \exp(-ikn_0Z)]$ is the solution of the reduced wave equation. Second derivatives of U in the propagation direction (Z) have been dropped in equation 33. The index of refraction difference term $(n^2-n_0^2)$ is approximated well by $2n_0n_1$, where $n = n_0 + n_1$, n_0 being the index of refraction of the quiescent gas (for air $n_0 \simeq 1.000292$). Using either the Gladstone-Dale relation for gases or the Lorentz-Lorenz relationship, one gets $n_1 = (n_0 - 1)\,\rho_1/\rho_0$, where density has been written as $\rho = \rho_0 + \rho_1$, ρ_0 being the quiescent gas density.

The density perturbation for the case of a constant transverse wind, v_0, can be determined by linearizing the appropriate hydrodynamic equations. Under the assumption that $v_0 \ll c_\infty$ where c_∞ is the speed of sound in the gas, the process can be shown to be isobaric. The density perturbations given by

$$\frac{\rho_1(x,y,z)}{\rho_0} = -\frac{(\gamma-1)}{\gamma\, v_0\, p_0} \int_{x-v_0 t}^{x} dx'\, \rho_0 \dot{Q}(x',y,z) \tag{34}$$

where $\rho_0\dot{Q}(x,y,z)$ is the laser heat deposition term. p_0 is the ambient pressure and is taken as constant in this analysis. Time (t) is measured from the instant the laser is turned on, although the solution is really only valid for times long compared to the acoustic transit time. In steady state ($t \to \infty$), the lower limit of the integral can be set to minus infinity.

The heat deposition term is a function of the radiation wavelength and its specific atomic or molecular absorption-thermalization process in air. If pure, instantaneous heating is assumed (as is the case for absorption of 10.6μm radiation by water), equation 34 is just

$$\frac{\rho_1(\bar{r})}{\rho_0} = -\left(\frac{\gamma-1}{\gamma}\right) \frac{\alpha}{v_0\, p_0} \int_{-\infty}^{x} I(x',y,z)dx' \tag{35}$$

where α is the absorption coefficient for the specific absorption-thermalization process being considered.

For the case of 10.6μm radiation, carbon dioxide in addition to water vapor is also found to be a strong absorber in the atmosphere. The absorption process is between the lower and upper lasing vibrational energy levels (10°0 and 00°1). The vibrational energy level diagram which is important to the absorption of 10.6 μm radiation by CO_2 is shown in figure 18. Briefly, the absorption energetics are the following (ref. 43). Upon absorption of a photon of 10.6μm radiation, the CO_2 vibrational system is raised from the (10°0) state to the (00°1) energy level. To raise a CO_2 molecule to this level, energy ε_{001} must be added to the system. A portion of this energy comes from the 10.6μm photon, the remaining portion coming from the energy in the (10°0 vibration level (ε_{100}). The (10°0) energy level is now no longer in thermal equilibrium and therefore, through collisional

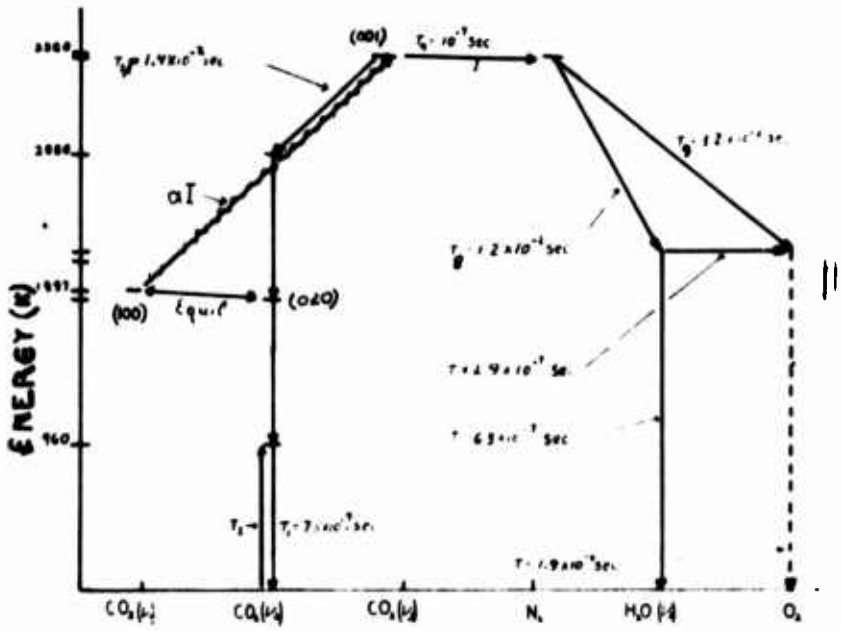

Figure 18. Vibrational Energy Level Diagram of Molecular Species Important to the Kinetic Processes of CO_2 Absorption of 10.6μm Radiation (ref. 43).

deactivation, it is repopulated by taking energy out of the translational energy (temperature) reservoir.

The process is very quick and engenders an immediate decrease in the temperature of the gas. Of course, this condition cannot last forever. Energy has been absorbed by the gas, and ultimately there must occur a temperature rise. This occurs in the following way. The (00°1) level of CO_2 is in near equilibrium with the first vibrational energy level of nitrogen. In the atmosphere there are roughly 2600 times as many nitrogen systems as CO_2 systems. Through collisional deactivation, most of the energy stored in the (00°1) CO_2 systems is quickly transferred to the nitrogen systems. The reverse reaction is effectively much slower because of the preponderance of the nitrogen molecules to carbon dioxide molecules. The excited nitrogen atoms can also return to ground through collisional deactivation with H_2O or O_2. All these rates are slow, however, producing in effect a freezing of the energy in the nitrogen vibrational energy reservoir. Thus, until nitrogen releases its energy, the effect of absorption of 10.6μm radiation by CO_2 is to cool the air. In the case of a wind, the extent to which a parcel of air is cooled or heated by the CO_2 absorption process depends on the length of time that the parcel is in the beam and the net relaxation rate of nitrogen.

Considering the two main sources of 10.6μm absorption (H_2O and CO_2), one can obtain for the density variation of equation 35

$$\frac{\rho_1(\bar{r})}{\rho} = -\alpha\left(\frac{\gamma-1}{\gamma}\right) \cdot \frac{1}{v_o\, p_o} \int_{-\infty}^{x} \left\{1-\sigma\exp\left[-\frac{(x-x')}{v_o\tau}\right]\right\} I(x',y,z)\,dx' \qquad (36)$$

where

$I(x,y,z)$ = irradiance distribution of the laser

τ = net relaxation rate of nitrogen

$\alpha = \alpha_{H_2O} + \alpha_{CO_2}$

$$\sigma = \left(\frac{\varepsilon_{001}}{\varepsilon_{001} - \varepsilon_{100}}\right)\frac{\alpha_{CO_2}}{\alpha} \simeq 2.441\ \frac{\alpha_{CO_2}}{\alpha}$$

Note that when $\tau = 0$, then $\frac{\rho_1}{\rho_o} = 0$; i.e., no cooling can occur. Similarly, if $\alpha_{CO_2} \simeq 0$, then $\sigma \simeq 0$ and again no cooling can occur. In general, neither of these conditions occurs in practice, so that the integrand of equation 36 may, under the appropriate conditions, assume negative values, thus indicating a cooling phenomenon. Sigma (σ) assumes its largest value (2.441) when $\alpha_{H_2O} \simeq 0$, so that the kinetic cooling phenomenon (as it is sometimes called) can be expected to occur at the higher altitudes in the atmosphere where the water vapor content is small. Finally, it is clear that no kinetic cooling can occur if $\alpha_{H_2O} > 1.44\ \alpha_{CO_2}$, though partial cooling can offset to some degree the heating due to absorption by H_2O.

Prior to the full diffraction treatment of thermal blooming (equation 28) extensive work on this subject was also performed using geometrical optics (refs. 39, 44, and 45). The full diffraction approach to the problem was later found necessary however, in order to adequately describe focused beams and cases of severe ray deflections (leading to caustics in geometrical optics).

Figure 19 is an example calculation of a diffraction code. The results are typical of focused beams with a constant transverse wind. Pure heating is assumed. Notice that the beam is deflected into the wind and that a crescent, or sugar scoop, irradiance profile develops. The amplitude in each frame has

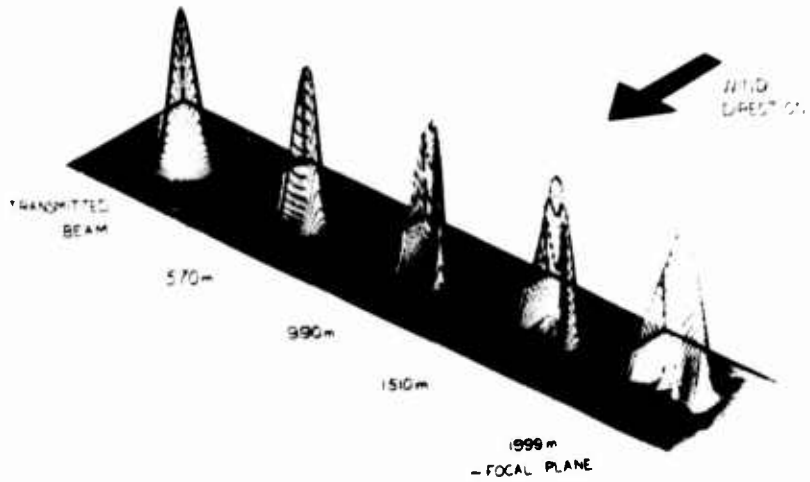

Figure 19. Typical Example of a Theoretical Computer Calculation of Thermal Blooming (ref. 36).

been normalized to unity. Again, it is reiterated these are steady state results (i.e., the beam is assumed to have been in for a long period of time).

The inclusion of kinetic cooling in the calculations can dramatically alter the focal plane irradiance distribution. For example, in figure 20, a typical focal plane irradiance distribution is seen when τ = 0 (pure heating). In figure 21, the same case is shown when τ = 15 msec. With kinetic cooling present, the beam is seen to deflect downwind, develop an irradiance distribution which appears to be self-trapping to some degree, and exhibit a peak irradiance which is better than twice as large as for the purely heating case. This latter characteristic, in fact, seems to be generally true. Whenever any degree of kinetic cooling is present, far-field maximum irradiance values are always improved over the comparable pure thermal blooming case.

In this vein, however, it should be pointed out that Sica (ref. 46) at the Naval Research Lab (NRL) has recently found experimentally that the earlier published values for the nitrogen relaxation rate are too large. Specifically, in the limit of very little water content, Sica's experimental measurements tend to agree with the theoretical published values. However, for larger water-vapor levels, the published values appear to be as much as six times larger than the experimental measurements. Generally speaking, however, for high-altitude 10μm propagation, this does not noticeably alter any previous conclusions because there is usually a sharp decrease in water vapor content with altitude (figure 22).

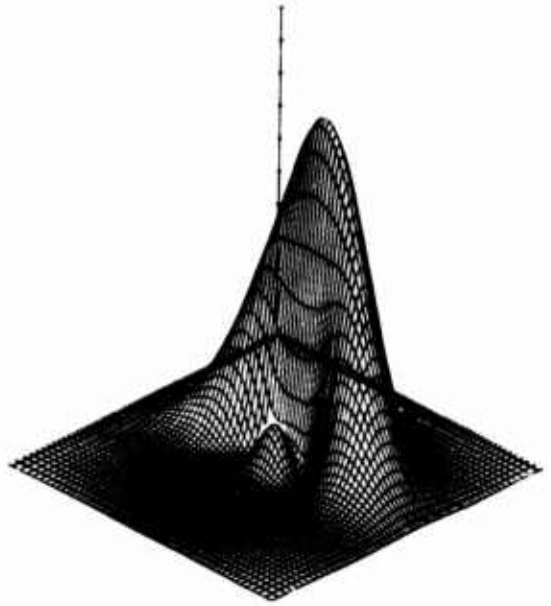

Figure 20. Characteristic Thermal Blooming Irradiance Profile for a Purely Heating Medium.

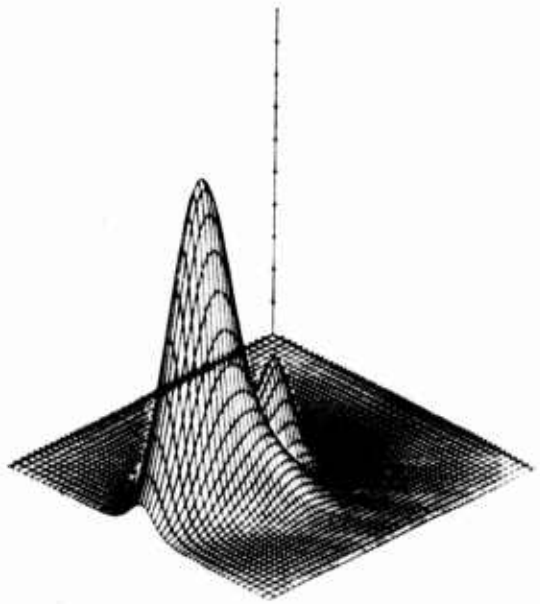

Figure 21. Characteristic Kinetic Cooling Irradiance Profile for a Dominatly Cooling Medium; Wind Is in the Same Direction for Both Figures 20 and 21.

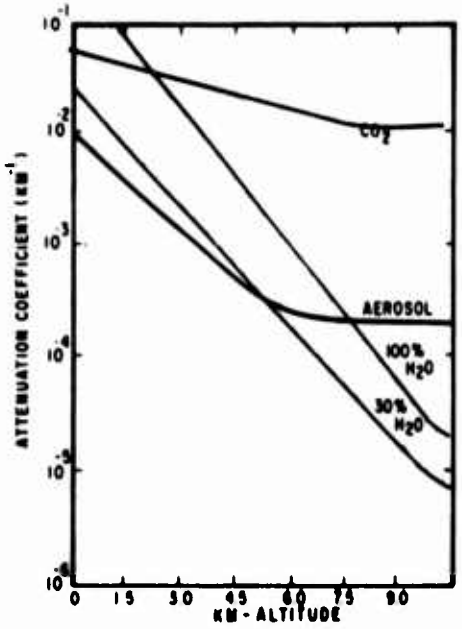

Figure 22. Attenuation of 10.6μm Radiation in the Air (ref. 43).

3. RESULTS AND STUDIES DEVELOPED FROM THE BASIC PROBLEM

In dealing with nonlinear problems one of the most difficult tasks is arriving at good scaling laws. By doing this, however, one can circumvent the usual time-consuming operation of numerical integration of equation 34 for each and every specific case of interest.

To approach such a problem one must know the parameteric dependencies of the specific variables of interest. Analysis of the governing equations frequently helps, but since the process is nonlinear, some care must be exercised with this approach. In this section some studies which have been conducted to investigate the parametric dependencies of thermal blooming are described.

a. Power Optimization

Solving equation 33, one finds that with increasing output power, the maximum irradiance in the receiver plane first begins to increase, gradually saturates, and then actually begins to decrease with yet larger power. This characteristic of the problem has lead to a group of parametric studies called power optimization curves. In figure 23, a sample power optimation study is shown with results obtained from numerically solving equation 33. Notice that the peak maximum power varies strongly, as does the corresponding optimum power setting for different absorption coefficients. Note also that these curves are for one fixed wavelength, one fixed transmitting aperture diameter, and one fixed

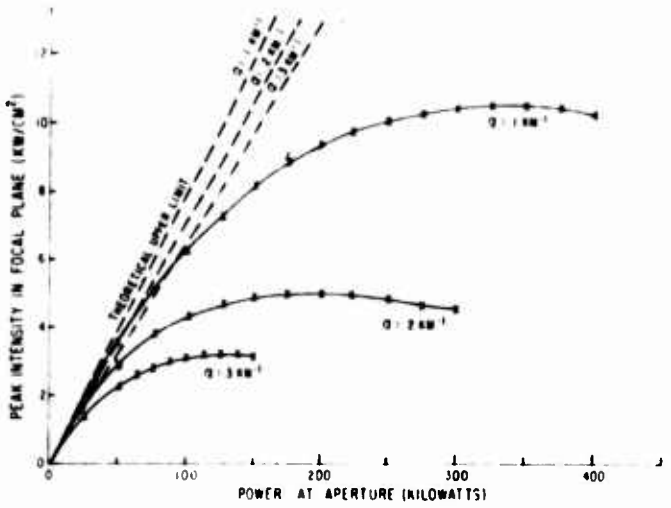

Figure 23. Thermal Blooming Power Optimization Curves (John Hayes, NRL, 1973).

focal length. Altering any of these can also drastically change the location (total output power) and magnitude of the focal plane maximum power.

Studying curves like these, Hayes and others at NRL were able to reliably fit all computed calculations for a fixed wavelength and aperture size to a function of the form

$$I_{peak}(f) = \frac{I_{vac}(f)\, e^{-\alpha f}}{1 + A(\alpha,f)\left(\frac{\alpha P_T}{V_0} e^{-\alpha f}\right) + B(\alpha,f)\left(\frac{\alpha P_T}{V_0} e^{-\alpha f}\right)^2} \qquad (37)$$

where $A(\alpha,f)$ and $B(\alpha,f)$ are polynomial functions in α and f (f is the focal length). The solid line in figure 23 is the parametric curve obtained with equation 37. From a consideration of the form of equation 36, one can deduce that blooming should scale in some fashion with quantities like $(\alpha\, P_T/V_0)$ and (αz). This is clearly reflected in equation 37.

Other parameters which appear in the analysis and may be good scaling quantities are

$\frac{f}{2\omega}$ = f/number

$\frac{\pi\omega^2}{\lambda f}$ = Fresnel Number

$N_f = (n_o - 1)\left(\frac{\gamma - 1}{\gamma}\right)\left(\frac{\alpha P_T}{v_o}\right)\left(\frac{z^2}{p_o \omega_1^3}\right)\left(\frac{\omega_1}{\omega f}\right)$ a dimensionless parameter developed by Gebhardt and Smith (ref. 38)

b. Parametric Dependence on Transmitted Beam Diameter and Wavelength

To deduce other scaling laws, one needs to study the additional effects of apertures and radiation wavelength on the thermal blooming process. Figure 24 is an example of the wavelength dependence of the process. Holding all else constant for each curve (α, ω, P_T, f, v_o), the wavelength of the radiation source was varied. The dashed curve shows the ideal limit of maximum irradiance versus wavelength. The solid curves lying below this are for different absorption coefficients. For ($\alpha P_T/v_o$) $\geq$ 0.9 watt-sec/m^2, the curves show an increase in focal plane irradiance with decreasing wavelength at a rate that is much less than the theoretical limit of λ^{-2}. In figure 25 the same data (normalized to the vacuum intensity) plus other data as well are plotted (on log-log scales). The limiting slope for decreasing wavelength is seen to be -1.54. Since $I_o(\lambda) \propto \lambda^{-2}$, then for this set of conditions, one can conclude that $I_{max} \propto \lambda^{-0.46}$, when $\alpha \geq 5\times10^{-5}$ m^{-1}. Note that figure 25 shows data for other transmitter aperture sizes as well, and that all the data reflects the above wavelength dependence.

In a similar fashion, figure 26 shows a parametric study of transmitting aperture dependence. Again the dashed line is the theoretical limit increasing as ω^2. The thermal blooming results lie below this curve and show an interesting result. As the transmitter aperture is increased. the focal plane irradiance in the presence of thermal blooming increases with an aperture dependence much the same as the aperture dependence of the vacuum propagation case. Figure 27 is a log-log plot of the relative irradiance, and shows a slop of approximately 0.5. For short wavelengths (these results were for λ = 10.6 m), the approximate same behavior is found to occur, with perhaps a slight increase in the slope with decreasing wavelength. These results suggest that for this situation, the focal plane irradiance maxima varies as $I_{max} \propto \omega^{2.5}$.

From these results, one must conclude that if all else is held constant, the far-field irradiance maximum is increased more by doubling the aperture size

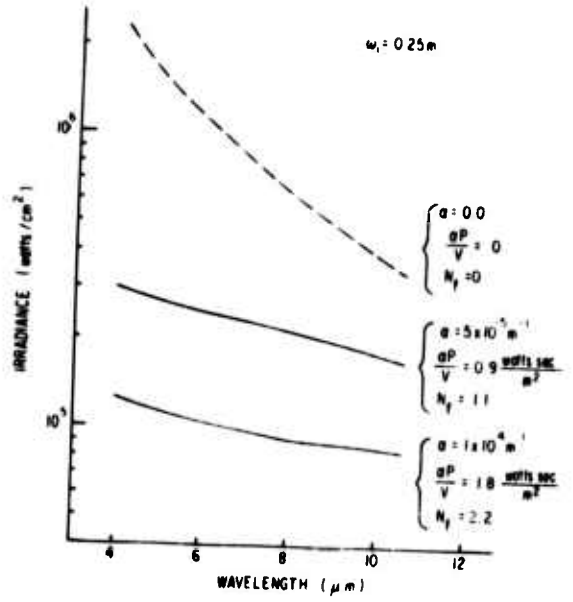

Figure 24. Wavelength Dependence of Thermal Blooming; Absolute Irradiance (peak) in Focal Plane.

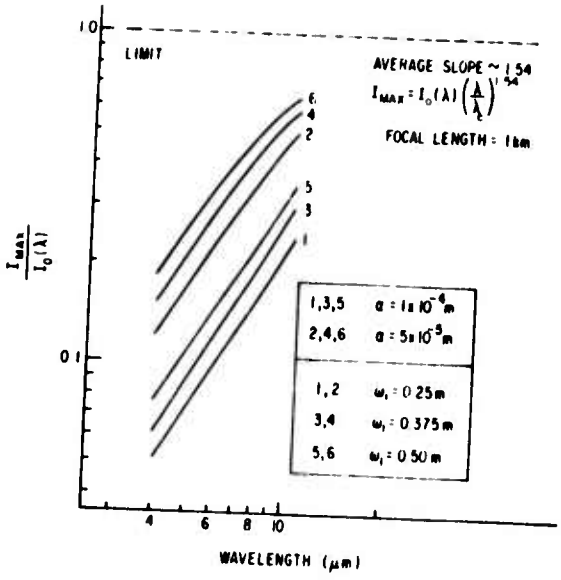

Figure 25. Wavelength Dependence of Thermal Blooming; Relative Irradiance (peak) in Focal Plane.

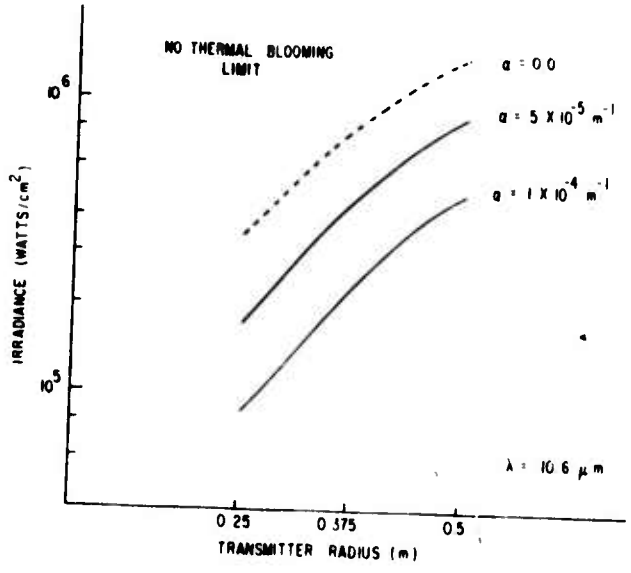

Figure 26. Aperture Dependence of Thermal Blooming; Absolute Irradiance (peak) in Focal Plane.

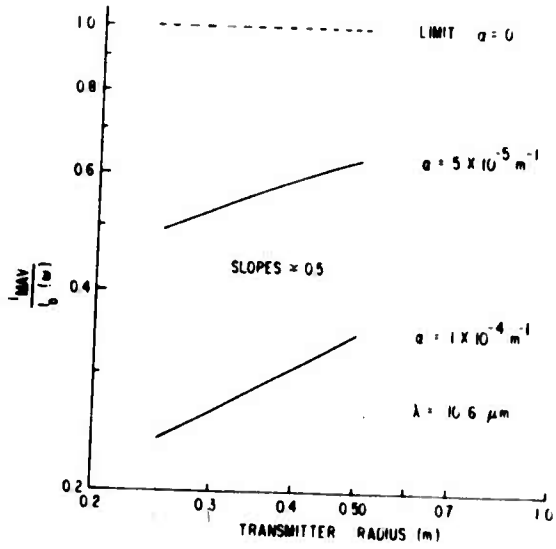

Figure 27. Aperture Dependence of Thermal Blooming; Relative Irradiance (peak) in Focal Plane.

than by halving the radiation wavelength (which for the vacuum propagation case would produce identical focal plane results). In fact, with increasing aperture size, the maximum irradiance actually begins to approach the diffraction-limited irradiance, whereas with decreasing wavelength, the maximum irradiance actually diverges from the limiting value. The reason for this behavior is two-fold. First, the shorter wavelength radiation is affected more strongly by comparable density gradients (as with turbulence) than the longer wavelength radiation. Second, the shorter wavelength radiation exhibits spot sizes at all points along the beam that are, in the vacuum limit, smaller than the longer wavelength spot sizes (for the same transmitter diameter, of course).

Therefore, for a constant output power, higher intensity levels result. This is true also for larger aperture systems for planes near the focal plane. However, at the other planes along the propagation axis that are slightly removed from the focal plane, the shorter wavelength system, at fixed transmitting aperture size, still has larger irradiance values than a longer wavelength system operating with very large transmitting optics. The situation is shown in figure 28, where the shorter wavelength (λ_1) and larger aperture size (ω_2) have been chosen to make the focal plane vacuum spot sizes the same for the two beams (i.e., $\lambda_1/\lambda_2 = \omega_1/\omega_2$). Thermal blooming is a nonlinear process that is driven solely by the form and magnitude of the laser beam irradiance distribution. Hence, one would therefore expect that for two vacuum equivalent systems (focal plane irradiance distributions), one with a large aperture and the other with a short radiation wavelength, that less thermal blooming would occur in the former case.

A related subject pertaining to this problem is the following. What portion of the propagation path contributes most to the thermal blooming phenomenon? In general, this is a complex question, the answer depending strongly on all the parameters. However, some things can be concluded. First, for a collimated beam (or diverging beam) it is easy to show that the maximum weight occurs at the transmitter. Here the density gradients are the largest and the propagation lever arm (to any observation plane) the longest. For the case of a focused beam in a constant transverse wind, the maximum contribution to thermal blooming no longer occurs in the vicinity of the transmitter. Two competing mechanisms, (1) the strength of density gradients and (2) the remaining propagation level arm, move the maximum of the weighting function away from the transmitter and nearer the focal plane--surprisingly near to the latter.

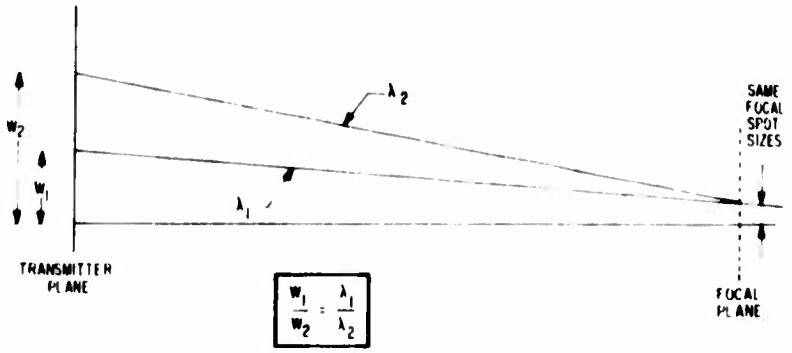

Figure 28. Simplified Explanation of the Wavelength Dependence and Transmitting Aperture Dependence on Thermal Blooming.

One can do a number of things to try to study this problem, but one of the clearest presentations of the effect can be seen if the following is computed. Consider a slice of propagation path which is, for example, 1/5 or 1/10 the total path length. Make this slice of path absorbing with some absorption coefficient α. Specify the rest of the propagation path to have a zero absorption coefficient (i.e., free space). Now place the absorbing segment at different positions between the transmitter and receiver and note the reduction in maximum irradiance. In figure 29, the results of performing this computation with a segment 200 meters long are shown; the focal length was 1 kilometer and the transmitting aperture diameter was 30 centimeters. The abscissa locates the center of the segment along the propagation path, and the ordinate presents the obtained relative irradiance for each case. The greatest reduction in irradiance occurs for a segment located between 700 and 800 meters. Shortening the segment length to 100 meters improves the resolution of this process, and these results are shown in figure 30. Apparently, the maximum weighting occurs near the 800-meter point.

To check the understanding of this process, a similar arrangement with a smaller transmitting aperture diameter of 20 centimeters was considered. The maximum of the weighting function should move toward the transmitter, and it does (figure 31). It must be pointed out, however, that the difficulty with using this sort of an analysis to locate the maximum weighting location is that the effects of accumulated optical distortions are not accurately assessed. Other work done by the author seems to indicate that for each of these cases a better estimate of the location of the weighting function maxima is actually slightly closer to the transmitter. Nonetheless, the conclusion is that for a focused beam, the portion of the optical path that contributes most heavily to the

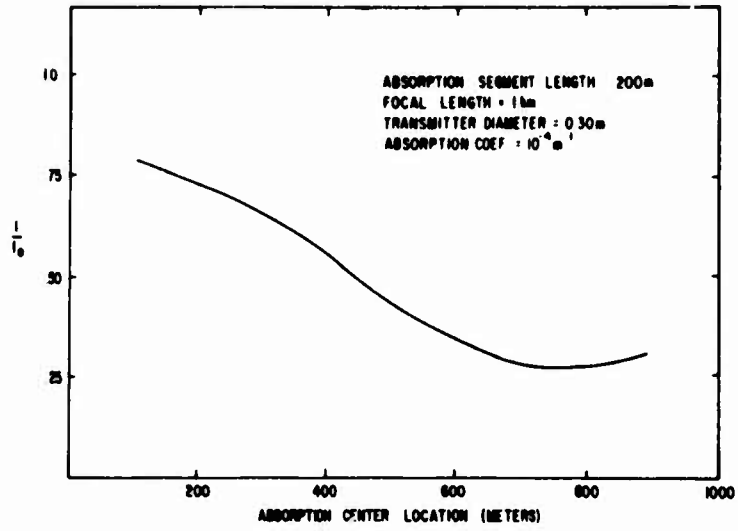

Figure 29. Relative Path Contribution to the Irradiance Degradation Casued by Thermal Blooming.

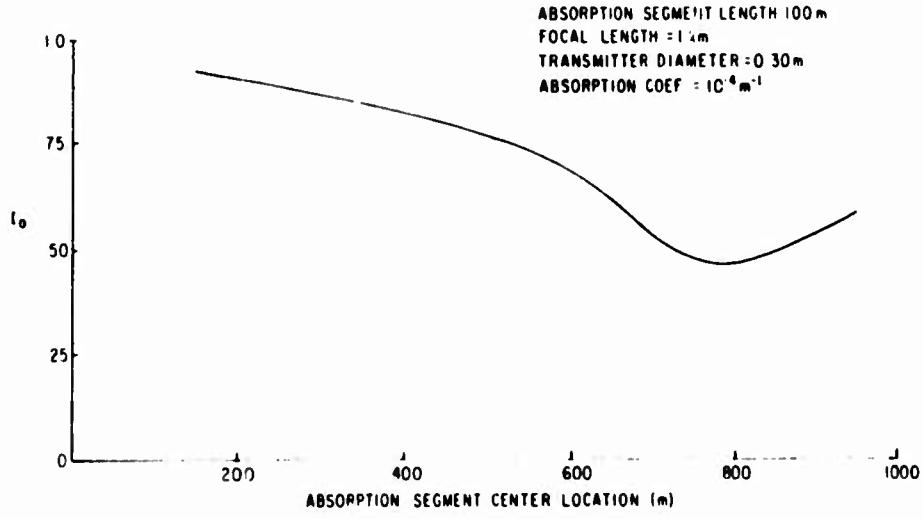

Figure 30. Relative Path Contribution to the Irradiance Degradation Caused by Thermal Blooming.

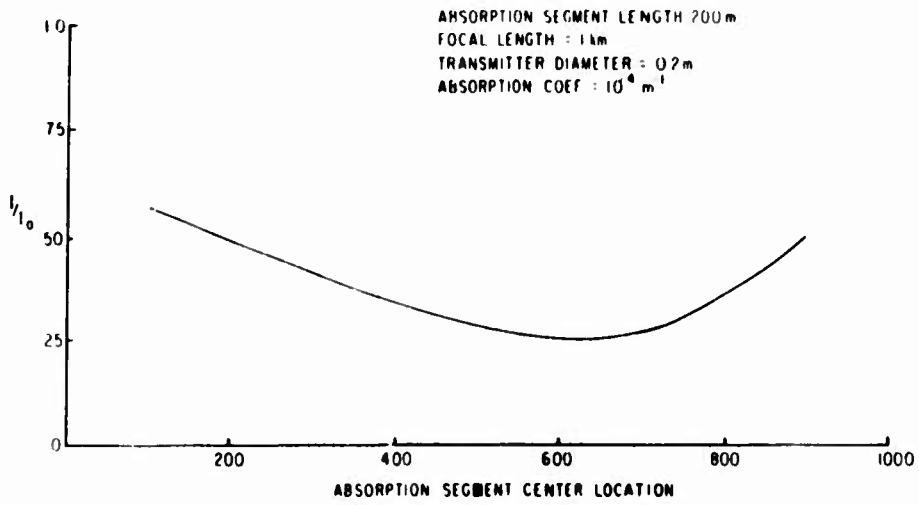

Figure 31. Relative Path Contribution to the Irradiance Degradation Caused by Thermal Blooming.

thermo-optical distortions is well away from the transmitter plane, and, in particular, for larger aperture transmitting systems, the position moves closer and closer to the receiver plane. This result obviously has some bearing on the explanation of the wavelength versus transmitter aperture size dependencies.

With the inclusion of slewing, wavelength-dependent absorption coefficients, etc., the preceding discussions must be somewhat re-evaluated. Nevertheless, the approach taken and some of the typical dependencies of the various parameters entering in the thermal blooming problem should be clear. Generally speaking, the problem is very complex and is made even more so by the necessity of treating special problems and effects which often occur.

4. SPECIAL PROBLEMS IN THERMAL BLOOMING

A number of interesting but specialized problems have developed as a result of the basic thermal blooming problem. One of the most obvious variations to the basic problem is the inclusion of an angular slewing velocity which has the effect of varying the transverse wind speed at points along the beam. At first thought, this seems to be a simple enough problem. However, it can create some very complicated situations. For instance, by simply slewing in a plane that does not lie parallel to the ambient wind direction, the wind transverse to the beam varies in magnitude and direction at all points along the beam. Generally speaking, this complicated situation has been neglected and the wind direction has been placed in the slew plane. If the slewing direction is into the wind and at all points along the beam the transverse wind is much less than Mach 1,

the thermal blooming problem can be treated quite well with a simple modification to the basic problem, namely by varying the transverse wind speed with range along the beam. However, two other problems of infinitely more complexity can occur if (1) the slew direction is reversed, and (2) if the slew rate is very large giving rise to transonic winds transverse to the beam. In the first case, if conditions are right, the slewing-induced wind and the naturally occurring wind can cancel one another, producing a situation where the wind transverse to the beam is zero (ref. 47). These are called "stagnation zones."

Analysis of the wind flow in the vicinity of stagnation zones is complex, and accurate computer modeling of even the simplest problems is very difficult (and approximate). Assuming that the air in the stagnation zone is truly stationary (which it usually is not) and making some assumptions with regard to the way in which the density gradients are modeled in this region, the irradiance distribution for a beam that has been on for 100 msec was obtained (the stagnation zone density variation growth is time dependent) and is shown in figure 32. The density gradient in the stagnation region acts as a negative lens, spreading the beam in all directions. In this case, the focusing effect of thermal blooming along the wind axis prevents the total divergence of the beam in that direction, thus resulting in a focal plane irradiance distribution that is double peaked in the direction normal to the wind. The strength of the effect varies as $(\alpha P/v_0\ \omega_1)$ for times longer than the acoustic transit time, although it is mitigated somewhat by the motion of the stagnation zone in space, or if it is not moving, then by the initiation of an induced convection wind, or both.

The second situation, that of a transonic flow, is a relatively new problem and is still being investigated (refs. 48, 49, and 50). The nature of the process can be visualized by looking at figure 33. Assume that at $t = 0$, the beam is in the position shown. The medium is continually absorbing energy, and therefore (approximately) cylindrical sound waves are constantly being generated. At $t = \Delta t$, the sound waves generated at $t = 0$ have reached the position shown by the dashed lines. At that time, the beam has reached the position shown. The intersection of the beam and the sound wave locates the position of transverse sonic wind flow. The result is that at this point in the beam, density perturbations grow into a shock wave across the leading edge of the beam. Depending on the nature of the medium and radiation, cooling or heating might be the dominant temperature effect. Whichever is the case, an underpressure or overpressure

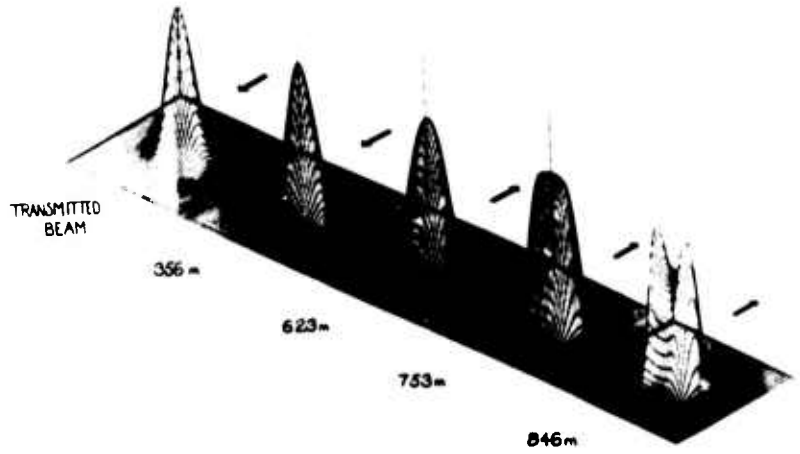

(a)

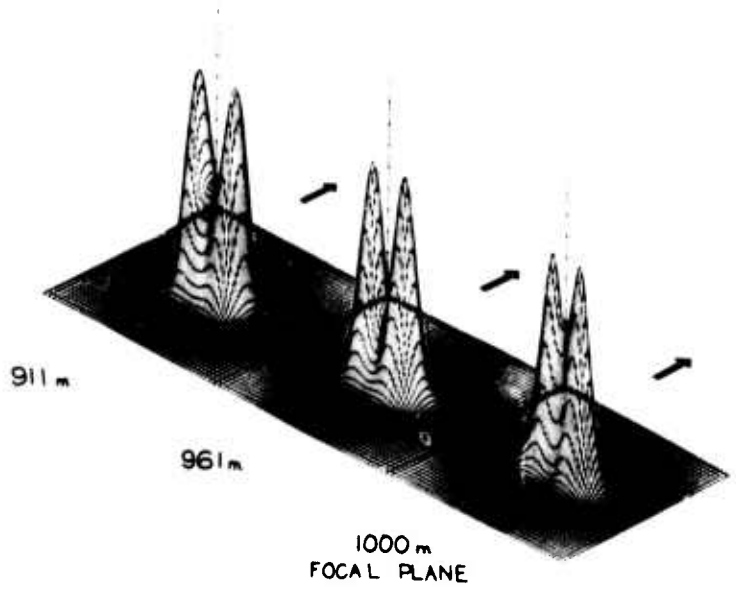

(b)

Figure 32. Thermal Optical Effects of a High-energy Beam Propagating Through a Stagnation Zone.

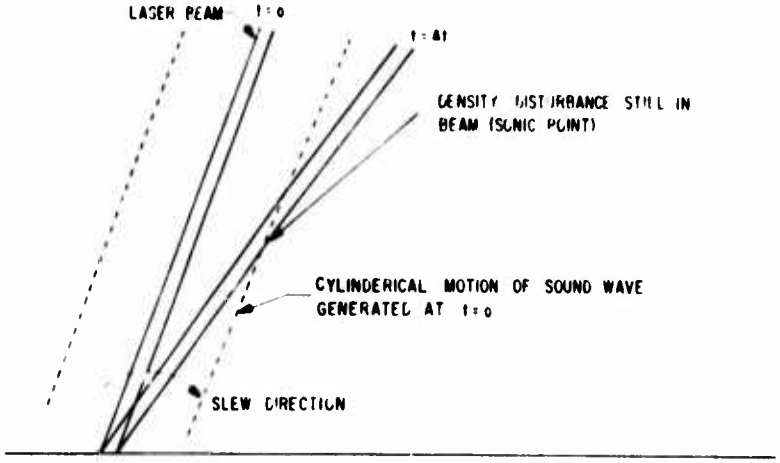

Figure 33. Simplified Graphical Description of the Source of Optical Degradation Arising From Transonic Winds.

Figure 34. Computer Calculations of Density Profiles Generated by a High-energy Beam with Transonic Transverse Winds.

shock wave, respectively, develops. Figure 34 shows three density profiles, one at Mach 1.1, Mach 1.0, and Mach 0.9, respectively, from left to right.

The first and the last profiles are steady-state solutions obtained from a two-dimensional hydro-code under the assumption of a Gaussian-shaped irradiance distribution (kinetic cooling dominated this case). The middle picture was obtained for the same conditions at a velocity of Mach 1. It is not a steady-state solution and is found to grow (after some initial millisecond transients) linearly in time. In figure 34 the plots are all normalized and consequently do not reflect the true relative magnitudes of the density gradients. Generally speaking, for a given time the density variations are always larger for the Mach 1 case than for velocities greater than or less than this. One finds that for velocity ranges other than Mach 1, the steady state density profile evolves in a time long compared to $2\ \omega(z)/|v_0-c_\infty|$, where the bars denote absolute value, and where $\omega(z)$ is the beam radius at the position z where v_0 is the transverse wind. Using these density profiles, a propagation configuration was modeled in which the Mach 1 velocity point occurred in the center of a 1-km path. The time evolution of the focal plane irradiance distribution is shown in figure 35 for a time up to 100 msec. In each frame the maximum irradiance has been scaled to unity.

Another class of problems deals with the effects of non-Gaussian and/or non-ideal phase profiles on thermal blooming. This category includes the study of apertured and obscured beams, nondiffraction limited beams (ref. 51), and beams propagating in the presence of atmospheric turbulence. Work is presently under way in all these areas. The problems are difficult, with the order of difficulty increasing as listed, respectively. Time does not permit a discussion of these problem areas.

Finally, there is the problem of short pulse propagation. Here one is concerned with pulse lengths whose duration is on the order of the hydrodynamic times; i.e., on the order of the acoustic transit time. The problem describes thermal blooming in the transient time region. This was purposely avoided in the treatment of the original basic thermal blooming problem. To simplify things slightly, it is usually assumed that during the pulse, the transverse motion of the air is negligible; that is, the wind is assumed to be zero, and thereby the problem is treated as a cylindrically symmetric one. The hydrodynamics can be solved exactly (for the linearized equations) if the irradiance distribution is assumed to remain Gaussian in shape throughout the entire pulse (which, to be

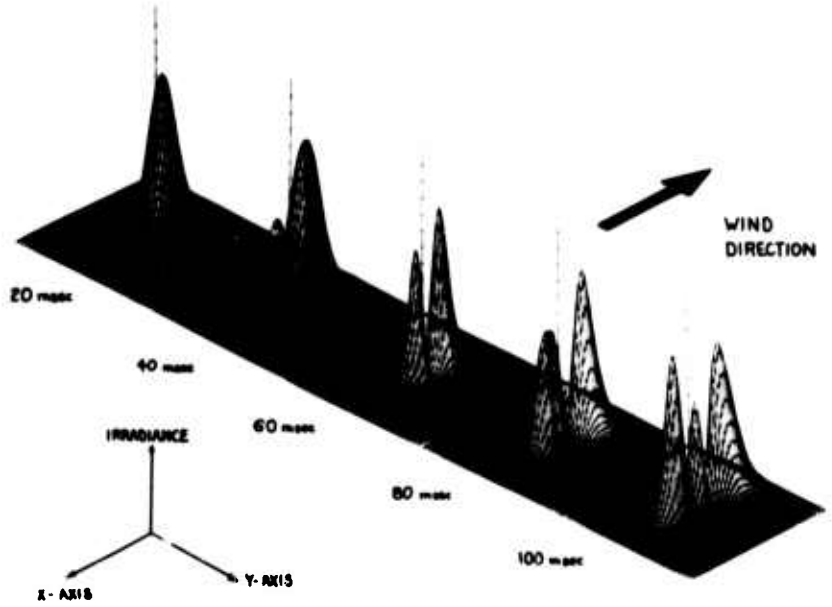

Figure 35. A Simulation of Optical Effects for a Beam Propagating Through a Transonic Region.

exact, it does not). One finds that the density initially grows for time (ref. 52) $t \ll t_{ac}$ ($t_{ac} = \omega/c_\infty$) as

$$\rho_1 = (\gamma-1)\,\alpha t^3\,\gamma^2\,I_0/6 \tag{38}$$

and for long times, $t \gg t_{ac}$, as

$$\rho_1 = \frac{-(\gamma-1)\,\alpha t\,I_0}{c_\infty^2} \tag{39}$$

where $I_0(r)$ is the Gaussian beam in a vacuum. For $t \ll t_{ac}$, a pressure wave is generated by the temperature rise (drop) which then propagates as an acoustic disturbance away from (toward) the beam. For times $t \gg t_{ac}$, the pressure is found to be constant, and the usual isobaric density growth occurs. In figure 36, one can see the propagation of the overpressure out of the beam (pure heating case), the later density changes being linear in t and proportional to the assumed irradiance profile of the laser (Gaussian).

For sufficiently high energy pulses, serious optical distortions can result. Figure 37 reproduces some of the results of Ulrich and Wallace (ref. 52) for the

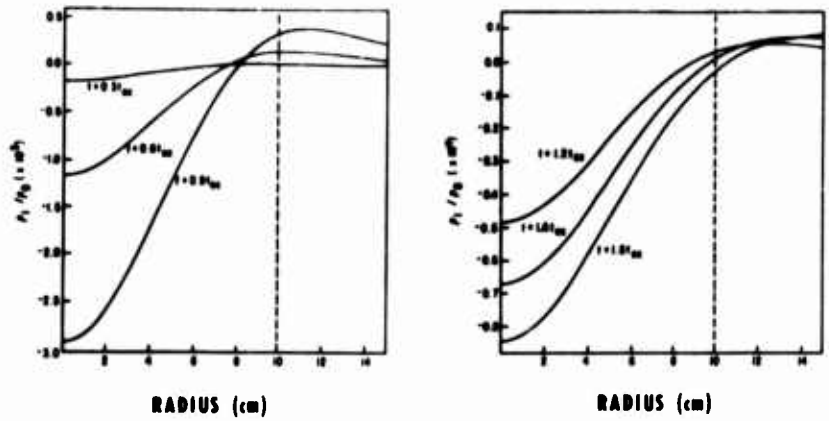

Figure 36. Transient Density Growth Caused by a Pulse of High-energy Laser Radiation (ref. 36)

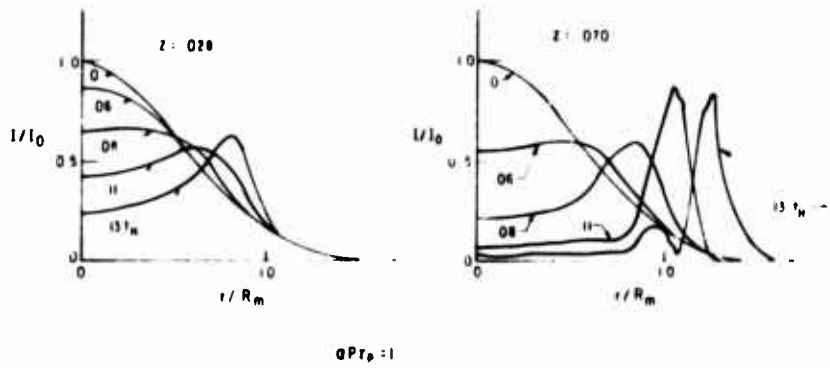

Figure 37. Blooming of a Pulsed, Collimated Beam (ref. 52).

propagation of a pulsed collimated beam. The range z is in units of Rayleigh range ($\pi\omega^2_{tr}/\lambda$) and times in fractions of t_{ac}. The results can be explained as follows. As air mass is moved out of the center of the beam in the compression wave, the local index of refraction decreases. Rays in the center of the beam are bent outward, redistributing the energy very quickly in an annulose shape. This effect was seen for the case where $t \gg t_{ac}$ in frame 2 of figure 16. For the longer range the optical distortions are more severe, the irradiance in the center of the beam going almost to zero.

Ulrich (refs. 53, 54, and 55) has also studied the propagation of pulsed, focused beams, and a typical result is shown in figure 38. The bottom figure is the time average of the upper figure results. Apparently, a donut-irradiance distribution can still form in the focal plane for a focused beam, but the magnitude of the outer ring seems to be reduced over the collimated beam result.

Ulrich has noted (personal communication) that for the case of pulsed, focused laser beams, the region along the propagation path which contributes most substantially to the thermo-optical distortions is near the focal plane. There are two reasons for this. One is that in this region, the density perturbations are the strongest, owing to the higher irradiance values obtained by focusing. The second reason is that because the beam is smaller (in diameter) here, the acoustic waves can be more rapidly propagated away from the beam, resulting in a more rapid density perturbation growth. Thus, even though the propagation lever arm is very short for these index-of-refraction disturbances, their magnitude is so strong that serious optical effects are still observed. Interestingly enough, this is in agreement with the earlier discussion of the range dependence of steady-state thermal blooming.

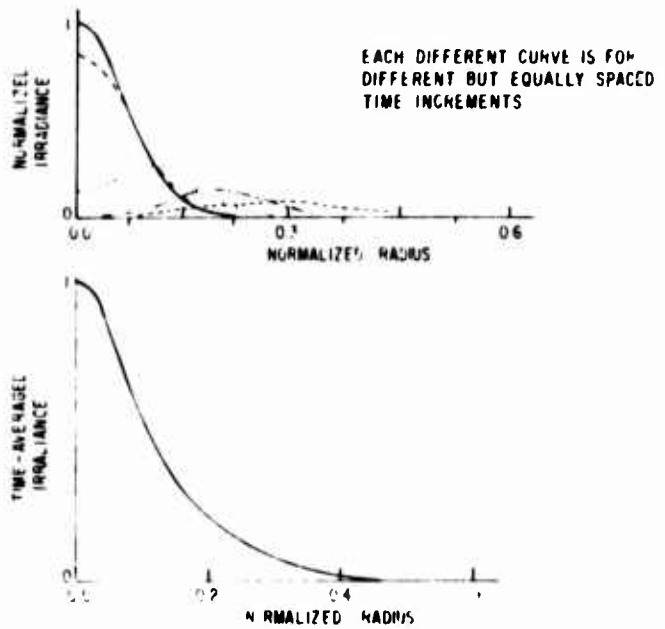

Figure 38. Blooming of a Pulsed, Focused Beam (ref. 54).

REFERENCES

1. Tatarski, V. I., Wave Propagation in a Turbulent Medium, Dover Publications, Inc. New York, 1961.

2. Chernov, L. A., Wave Propagation in a Random Medium, McGraw-Hill Book Company, Inc. New York, 1960.

3. Tatarski, V. I., The Effects of the Turbulent Atmosphere on Wave Propagation, Israel Program for Scientific Translations, Jerusalem, available from U. S. Dept. of Commerce, 1971.

4. Strohbehn, J. W., "Line of Sight Wave Propagation through the Turbulent Atmosphere," Proc. IEE, 56, 1301, 1968.

5. Lawrence, R. S. and Strohbehn, J. W., "A Survey of Clear-Air Propagation Effects Relevant to Optical Communications," Proc. IEEE, 58, 1523, 1970.

6. Lawrence, R. S., Ochs, G. R., and Clifford, S. F., "Measurements of Atmospheric Turbulence Relevant to Optical Propagation," JOSA, 60, 826, 1970.

7. Ochs, G. R., "Measurements of 0.63μm Laser-Beam Scintillation in Strong Atmospheric Turbulence," ESSA Tech Report ERL 154-WPL 10, 1969.

8. Ochs, G. R. and Lawrence, R. S., "Saturation of Laser-Beam Scintillation under Conditions of Strong Atmospheric Turbulence," JOSA, 59, 226, 1969.

9. Kerr, J. R., "Experiments on Turbulence Characteristics and Multi-wavelength Scintillation Phenomena," JOSA, 62, 1040, 1972.

10. Ochs, G. R. and Lawrence, R. S., "Saturation of Laser-Beam Scintillation under Conditions of Strong Atmospheric Turbulence," JOSA, 59, 226, 1969.

11. Ochs, G. R., Bergman, R. R., and Snyder, J. R., "Laser-Beam Scintillation over Horizontal Paths from 5.5 to 145 km, " Lett. JOSA, 59, 231, 1969.

12. Ishimaru, A., "Fluctuations of a Focused Beam Wave for Atmospheric Turbulence Probing," Proc. IEEE, 57, 407, 1969.

13. Lutomirski, R. F. and Yura, H. T., "Propagation of a Finite Beam in an Inhomogeneous Medium," Appl. Opt. 10, 1652, 1971

14. Yura, H. T., "Optical Beam Spread in a Turbulent Medium: Effect of the Outer Scale of Turbulence," JOSA, 63, 107, 1973.

15. Yura, H. T., "Short Term Average Optical Beam Spread in a Turbulent Medium," JOSA, 63, 567, 1973.

16. Heidbreder, G. R., "Image Degradation with Random Wavefront Tilt Compensation," IEEE, PGAP, 15, 90, 1967.

REFERENCES (Cont'd)

17. Moreland, J. P. and Collins, S. A., "Optical Heterodyne Detection of a Randomly Distorted Signal Beam," JOSA, 59, 10, 1969.

18. Fried, D. L., "Optical Resolution Through a Randomly Inhomogeneous Medium for Very Long and Very Short Exposures," JOSA, 56, 1372, 1966.

19. Hufnagel, R. E. and Stanley, N. R., "Modulation Transfer Function Associated with Image Transmission through Turbulent Media," JOSA, 54, 52, 1964.

20. Collins, S. A., Jr. and Damon, E. K., Angel of Arrival Calculations at 10.6 μm, RADC-TR-71-124, 1971.

21. Kerr, J. R. and Eiss, R. "Transmitter Size and Focus Effects on Scintillations," JOSA, 62, 682, 1972.

22. Dowling, J. and Livingston, P. M., "Behavior of Focused Beams in Atomospheric Turbulence: Measurements and Comments on the Theory," JOSA, Vol. 63, 846, 1973.

23. Kerr, J. R. and Dunphy, J. R., "Experimental Effects of Finite Transmitter Apertures on Scintillations," JOSA, 63, 1, 1973.

24. Hull, R. J., Gilmartin, T. J., and Marquet, L. C., Laser Beam Wander in Atmospheric Propagation, Project Report LTP-7, 1971.

25. Alcarey, E. C. and Livingston, P. M., Measurements of the Beam Wander Phenomenon in a Turbulent Medium, BRL-MR-2103, 1971.

26. Chiba, T., "Spot Dancing of the Laser Beam Propagated Through the Turbulent Atmosphere," Appl. Opt., 10, 2456, 1971.

27. Fried, D. L., "Statistics of a Geometric Representation of Wavefront Distortion," J. Opt. Soc. Am., 56, 1969.

28. Fried, D. L., "Optical Heterodyne Detection of an Atmospherically Distorted Signal Wavefront," Proc. IEEE, 55, 57, 1967.

29. Fried, D. L. and Yura, H. T., "Telescope Performance Reciprocity for Propagation in a Turbulent Medium," Lett. to JOSA, 62, 600, 1972.

30. Yura, H. T., "Atmospheric Turbulence Induced Laser Beam Spread," Appl. Opt., 10, 2771, 1971.

31. Lutomirski, R. F. and Yura, H. T., "Wave Structure Function and Mutual Coherence Function of an Optical Wave in a Turbulent Atmosphere," JOSA, 61, 482, April 1971.

32. Wallace, J., "Effect of Nonlinear Refraction at 10.6μm on the Far Field Irradiance Distribution," JOSA, 62, 373, 1972.

33. Wallace, J. and Camac, M., "Effects of Absorption at 10.6μm on Laser-Beam Transmission," JOSA, 60, 1587, 1970.

REFERENCES (Cont'd)

34. Hayes, J. N., Ulrich, P. B., and Aitken, A. H., "Effects of the Atmosphere on the Propagation of 10.6μm Laser Beams," Appl. Opt. 11, 257, 1972.

35. Livingston, P. M., "Thermally Induced Modivications of a High Power cw Laser Beam," Appl. Opt. 10, 426, 1971.

36. Hogge, C. B., Thermo-Optical Effects of High Energy Laser Beams, AFWL-TR-72-184, Air Force Weapons Laboratory, Kirtland AFB, NM, 1972.

37. Smith, D. C., "Thermal Defocusing of CO_2 Laser Radiation in Gases," IEEE J. QE. 5, 6000, 1969.

38. Gebhardt, F. G. and Smith, D. C., "Effects of Diffraction on the Self-Induced Thermal Distortion of a Laser Beam in a Cross-wind," Appl. Opt. 11, 244, 1972.

39. Gebhardt, F. G. and Smith, D. C., "Self-Induced Thermal Distortion in the Near Field for a Laser Beam in a Moving Medium, " IEEE J. QE. 7, 63, 1971.

40. Buser, R. G. Rhode, R. S., "Severe Self-Induced Beam Distortion in Laboratory Simulated Laser Propagation at 10.6μm," Appl. Opt. 12, 205, 1973.

41. Kenemuth, J. R., Hogge, C. B., Avizonis, P. V., "Thermal Blooming of a 10.6 μm Laser Beam in CO_2," Appl. Phys, Lett., 17, 220, 1970.

42. Ulrich, P. B., Hayes, J. N., and Aitken, A. H., "Comparison of a Wave Optics Computer Model with Nonlinear Propagation Experiments," JOSA, 62, 289, 1972.

43. Wood, A. D., Camac, M., and Gerry, E. T., "Effects of 10.6μm Laser Induced Air Chemistry on the Atmospheric Refractive Index," Appl. Opt. 10, 1877, 1971.

44. Avizonis, P. V., Hogge, C. B., Butts, R. R., Kenemuth, J. R., "Geometric Optics of Thermal Blooming, Part I," Appl. Opt, 11, 554, 1972.

45. Hayes, J. N., "Thermal Blooming of Laser Beams in Fluids," Appl. Opt. 11, 455, 1972.

46. Sica, L., "Interferometric Observations of Kinetic Cooling," USNRL, Appl. Phys, Lett., Vol. 22, 396, 1973.

47. Hogge, C. B. and Butts, R. R., Propagation Effects of a Slewed Beam with Transverse Wind Null Spots, AFWL-TR-73-76, Air Force Weapons Laboratory, Kirtland AFB, NM, 1973.

48. Hogge, C. B. and Brau, J. E., "Optical Effects of Transonic and Supersonic Winds on High Energy Laser Beams," AFWL-TR-73-131, Laser Division Spring Digest, Air Force Weapons Laboratory, Kirtland AFB, NM, 1973.

49. Brau, J. E. and Hogge, C. B., "A Comparison of One- and Two-Dimensional Models of Laser-Induced Density Anomalies in Flowing Air," AFWL-TR-73-131, Laser Division Spring Digest, Air Force Weapons Laboratory, Kirtland AFB, NM 1973.

REFERENCES (Cont'd)

50. Hayes, J. H., Thermal Blooming of Rapidly Slewed Laser Beams, NRL Tech Note, 1973.

51. Hogge, C. B. and Burlokoff, M., Thermal Blooming of Nondiffraction Limited Beams, AFWL-TR-73-77, Air Force Weapons Laboratory, Kirtland AFB, NM 1973.

52. Ulrich, P. B. and Wallace, J., "Propagation Characteristics of Collimated, Pulsed Laser Beams Through an Absorbing Atmosphere," JOSA, 63, 9, 1973.

53. Ulrich, P. B., A Numerical Calculation of Thermal Blooming of Pulsed, Focused Laser Beams, NRL Report 7382, 1971.

54. Ulrich, P. B., "Requirements for Experimental Verification of Thermal-Blooming Computer Results," JOSA, Vol. 63, 897, 1973.

55. Aitken, A. H., Hayes, J. H., Ulrich, P. B., "Thermal Blooming of Pulsed Focused Gaussian Laser Beams," Appl. Opt. 12, 193, 1973.